PROCEEDINGS OF THE ROYAL SOCIETY A

rspa.royalsocietypublishing.org

Research

Cite this article: Mora K, Budd C, Glendinning P, Keogh P. 2014 Non-smooth Hopf-type bifurcations arising from impact–friction contact events in rotating machinery. *Proc. R. Soc. A* **470**: 20140490. http://dx.doi.org/10.1098/rspa.2014.0490

Received: 22 June 2014
Accepted: 19 August 2014

Subject Areas:
differential equations, applied mathematics, mechanics

Keywords:
non-smooth bifurcation, rotor dynamics, impact with friction, magnetic bearing systems, Hopf-type bifurcation

Author for correspondence:
Karin Mora
e-mail: karin@mora-online.de

Royal Society Publishing

Non-smooth Hopf-type bifurcations arising from impact–friction contact events in rotating machinery

Karin Mora[1], Chris Budd[1], Paul Glendinning[3] and Patrick Keogh[2]

[1]Department of Mathematical Sciences, and [2]Department of Mechanical Engineering, University of Bath, Claverton Down, Bath BA2 7AY, UK
[3]Centre for Interdisciplinary Computational and Dynamical Analysis (CICADA) and School of Mathematics, University of Manchester, Manchester M13 9PL, UK

We analyse the novel dynamics arising in a nonlinear rotor dynamic system by investigating the discontinuity-induced bifurcations corresponding to collisions with the rotor housing (touchdown bearing surface interactions). The simplified Föppl/Jeffcott rotor with clearance and mass unbalance is modelled by a two degree of freedom impact–friction oscillator, as appropriate for a rigid rotor levitated by magnetic bearings. Two types of motion observed in experiments are of interest in this paper: no contact and repeated instantaneous contact. We study how these are affected by damping and stiffness present in the system using analytical and numerical piecewise-smooth dynamical systems methods. By studying the impact map, we show that these types of motion arise at a novel non-smooth Hopf-type bifurcation from a boundary equilibrium bifurcation point for certain parameter values. A local analysis of this bifurcation point allows us a complete understanding of this behaviour in a general setting. The analysis identifies criteria for the existence of such smooth and non-smooth bifurcations, which is an essential step towards achieving reliable and robust controllers that can take compensating action.

1. Introduction

In rotating machines that are levitated by magnetic bearings, non-smooth events involving impact and

friction can occur between a spinning rotor and a touchdown bearing (TDB), which has the function of protecting the rotor and other stator components. These events are undesirable as they may be destructive and hence costly [1]. For the rigorous derivation of possible control strategies, it is important to understand the resulting dynamics. Thus, it is essential to understand how periodic impacting motions arise through new types of non-smooth bifurcations, and the purpose of this paper is to study these. The dynamics of constrained mechanical systems experiencing (instantaneous) impact and/or friction contact events have been studied extensively in the literature using a variety of different approaches [2]. These include measure differential inclusions [3–7], complementarity methods [8] and also the use of non-smooth hybrid systems [8–13]. In the latter formalism, the evolution of such systems is described by a piecewise-smooth flow, interrupted by events such as instantaneous impacts described by maps, and is well suited for studying periodic impacting solutions and their bifurcations. These systems experience energy dissipation, which can be modelled by Newton's restitution law, also referred to as the kinematic model, and Coulomb's friction law [10,13–17]. In this paper, we adopt the hybrid system formalism to study the bifurcations of the periodic orbits of a simplified rotating machine, in which a spinning disc (rotor) moves in two dimensions and experiences instantaneous contact events with a rigid circular boundary (TDB). This system can be modelled as a two degree of freedom impact–friction oscillator. Although other energy dissipation models, such as Poisson's kinetic [18] or Stronge's energetic [12,19] model, can be adopted, all three models (kinematic, kinetic and energetic) are equivalent for this system due to the rotor's properties; we will elaborate the details in §2. The study of hybrid systems related to impacting problems has led to the identification and classification of many types of novel dynamics, including periodic and chaotic motions, much of which arises at discontinuity-induced bifurcations (DIBs) such as the boundary equilibrium bifurcation (BEB) [10,13,14]. In this paper, we identify a novel form of bifurcation, at which a pair of impacting limit cycles are created simultaneously at a BEB point, when a non-impacting equilibrium of the rotor motion lies on the boundary.

In general, the dynamic behaviour of rotating machines as described can be very complex. Simplified models that do not take rotor damping and/or stiffness into account have been studied in [20,21]. Li & Païdoussis [20] focus on numerically investigating continuous contact (rub) and repeated impact motion, which yields rich dynamics such as chaos as well as non-smooth bifurcations. Lu *et al.* [21] analytically derive existence conditions of periodically impacting motion. Our intention in this paper is not to give a complete survey of such, but to consider a specific form of motion and the novel Hopf-type bifurcations, which lead to this. In particular, Keogh & Cole [22] show that a rotor–stator system with damping and friction can exhibit various forms of stable and unstable synchronous single impact limit cycles. In this paper, we present a global analysis of the existence of this type of orbit and describe the novel bifurcations between the aforementioned equilibrium states without impact and *two* coexisting limit cycles with different period at the BEB point. This bifurcation has many of the qualitative features of a smooth Hopf bifurcation in that small amplitude impacting limit cycles of non-zero period are created close to the BEB point. For the sake of classification, we shall call it a *non-smooth Hopf* (*NSH*) *bifurcation*. Our analysis of this bifurcation will be general and applicable to many other related problems. Similar discontinuity-induced Hopf bifurcations, exhibiting a bifurcation of a non-impacting equilibrium to a limit cycle with impact, have been observed in planar piecewise smooth continuous systems [13,14,23] with sliding [24] and with biological applications [25]. In vibro-impacting systems of two degrees of freedom NSH bifurcations have been observed and can also be a route to chaos [15,16]. In the bifurcation analysis we present in this paper, when studying the effects of bearing damping, we also find two coexisting smooth fold bifurcations. Furthermore, we show the existence of orbits, which at the point of impact, have zero normal velocity and lie tangential to the impact surface, called *grazing* orbits [11].

The remainder of this paper is laid out as follows. In §2, we give a brief introduction to magnetic bearing systems comprising a spinning rotor with a disc cross section impacting with a TDB. We derive the non-dimensionalized equations of the disc in free flight and the reset law

describing the behaviour at impact. In §3, we give examples of the possible dynamics, i.e. the rotor motion in the absence of impact and under impact, and identify the impact map, which allows further analysis of the system. In §4, we apply a Poincaré (impact) mapping technique, which allows us to determine solutions corresponding to the simplest forms of periodically or quasi-periodically impacting orbits. The resulting global analysis yields new smooth and piecewise-smooth dynamics, including the existence of the NSH-type bifurcations describing the bifurcation from a non-impacting equilibria to two separate periodic orbits with impact. In §5, we present a more detailed (local) study of the NSH-type bifurcation, looking at a more general class of problems. The results of this analysis are then compared with the calculations of §4. Finally, in §6 we present our conclusions and suggest some open questions.

2. Introduction to magnetic bearing systems and their associated dynamics

(a) Overview

Rotating machines are prevalent in engineering applications that require power to be generated or used. The power rating is determined by the product of the driving or load torque and the rotational speed. In order to operate effectively, a rotor should spin in a stable manner under the support of bearings. The bearings should also be able to cope with inherent rotor unbalance and any fault conditions that may occur during operation of the machine. A number of bearing types are available to designers of machines, commonly including those based on rolling ball or cylindrical elements, and bushings with oil films. Usually, there is a specified maximum operating speed, below which it is safe to run the rotor. If this speed is exceeded for any significant period, the bearing is likely to fail due to high mechanical or thermal stresses. Gas bearings may allow higher speed operation, but they are limited in their load carrying capacity and require a continuous flow of pressurized air. Foil/gas bearings are self-acting and do not require a pressurized source, though below a threshold speed the foil element is in rubbing contact with the rotor and is then prone to wear.

Active magnetic bearings (AMBs) have been under development since the 1970s and have seen a growing number of applications including in turbomolecular and vacuum pumps, compressors, motors, generators, centrifuges, flywheels and beam choppers. An arrangement of electromagnets under feedback control enables a rotor to be levitated. It may then rotate without direct interaction with bearing surfaces or fluids, which has advantages in terms of friction reduction and the elimination of the need for pressurized oil or gas supplies. Higher operating speeds are therefore possible. However, magnetic bearing functionality may be compromised by failure of the power supply, which would lead to rotor delevitation. Also, any external disturbance may cause the load capacity of the bearing, which is limited by magnetic flux saturation, to be exceeded. Magnetic bearings may be configured to transmit low forces at a particular operating speed, through use of a notch filter in the feedback control, but high acceleration input disturbances, e.g. shock conditions, would be problematic. For these reasons, magnetic bearings usually contain secondary TDBs to prevent rotor motion from exceeding damaging limits. The design issues for such systems are given in [26].

Although some studies have been made to investigate the nonlinear rotor dynamics that arise from rotor contact with TDBs, the problem is still not completely understood. The condition for backward whirl, which may involve severe contact forces, is understood as the condition in which the rotor is in rolling contact with the TDB [22]. A number of authors have considered the dynamics of a rotor within a clearance space [27–39]. With respect to operational magnetic bearing systems, which is in contrast to complete delevitation, it is important to gain a full understanding of all nonlinear dynamic issues so that appropriate control action may be designed to recover contact-free levitation. Without this knowledge, it is not possible to ensure that normally levitated control is recoverable.

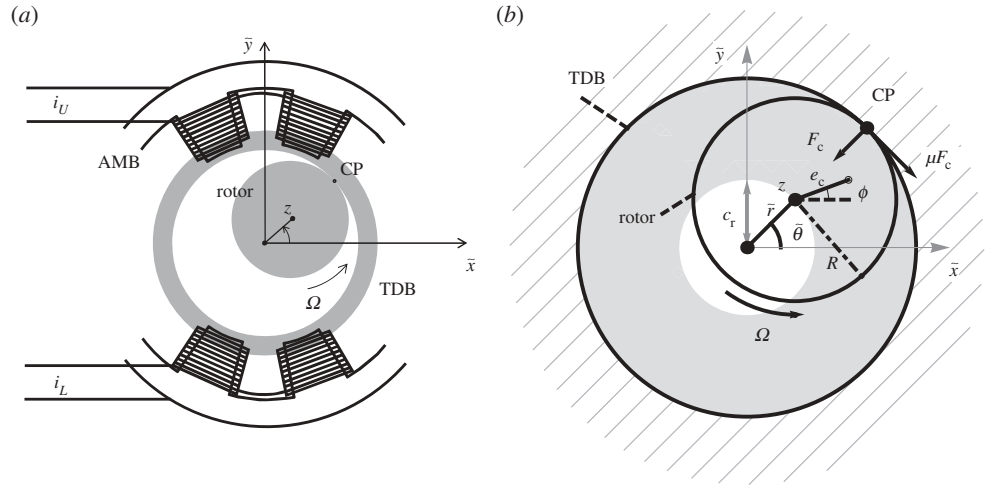

Figure 1. Fixed Frame: (*a*) The AMB currents, i_U and i_L, are shown in the vertical axis only. With appropriate control, these determine the AMB stiffness and damping characteristics. (*b*) The rotor-TDB impact is at the contact point CP; contact force F_c and frictional force μF_c are acting. The rotor centre is shown in both complex coordinate z and polar coordinates $(\tilde{r}, \tilde{\theta})$. In free flight, its motion is constrained to be within the clearance disc (white). The rotor is affected by mass unbalance with eccentricity e_c and phase angle ϕ.

(b) Free motion

The mechanical model, illustrated in figure 1, is adopted from [22]. It comprises a rotor, with a disc cross section of radius R, spinning at a high constant speed, $\Omega > 0$, inside a fixed, circular TDB. At the bearing centre lies the origin, from which we define the rotor position (disc centre) in polar coordinates $(\tilde{r}, \tilde{\theta})$. The rotor comes into contact with the bearing when $\tilde{r} = c_r$, where c_r is the radius of the clearance circle. We study the motion of the rotor centre without impacts, i.e. if $\tilde{r} < c_r$, and with impacts, i.e. if $\tilde{r} = c_r$. For convenience, we describe the position of the rotor centre z at time τ using complex coordinates in the form

$$z(\tau) = \tilde{x}(\tau) + \mathrm{i}\tilde{y}(\tau) = \tilde{r}(\tau)\,\mathrm{e}^{\mathrm{i}\tilde{\theta}(\tau)}. \tag{2.1}$$

The system under consideration has magnetic bearing support characteristics under *proportional-integral-derivative* (PID) control. Then the rotor's motion can be approximated by a linear spring-damper system with stiffness k and damping c [22]. For real machines the integral (I) gain would be typically set at a level that gives rise to a dynamic mode having a very long time constant. Thus, when the magnetic bearing is activated the integral action ensures that the rotor rises slowly to the bearing centre. Thereafter, it is common to set the integral gain to zero and the established control currents will continue to levitate the rotor at the bearing centre. The remaining proportional (P) and derivative (D) gains will then cause the spring-damper terms to be effective when the rotor deviates from levitated equilibrium at the magnetic bearing centre. In addition, the rotor, of mass m is affected by mass unbalance with force f_u. In free flight the rotor centre z, (2.1), lies within the clearance circle of radius c_r and satisfies a linear constant coefficient complex valued ODE,

$$m\ddot{z}(\tau) + c\dot{z}(\tau) + kz(\tau) = f_u\,\mathrm{e}^{\mathrm{i}\Omega\tau} \quad \text{if } |z(\tau)| < c_r. \tag{2.2}$$

The forcing term depends on the angular speed Ω as well as the complex unbalance force f_u, which is given by

$$f_u = me_c\Omega^2\,\mathrm{e}^{\mathrm{i}\phi},$$

where e_c is the unbalance eccentricity (distance between geometric centre and centre of mass) and the unbalance phase ϕ (figure 1).

(c) Motion with impacts

The motions of the rotor, studied in this paper, are piecewise-smooth orbits. These orbits comprise smooth trajectories satisfying a smooth differential equation, which are interrupted by instantaneous collisions. The collisions or impacts lead to non-smooth changes in the system velocities (but not its position) as governed by reset laws. There is a range of designs for practical TDBs, including bushing and rolling element types. These are mounted in housings, either directly as push fits or with some compliant backing material to provide some degree of cushioning. A rotor mounted touchdown sleeve may be included as another component. However, a requirement is that the rotor motion must be constrained sufficiently so as to protect the rotor and magnetic bearing. This necessitates that the radial stiffness associated with a TDB must be significantly greater than that associated with a magnetic bearing [1,40,41]. Any contact between a rotor and TDB will generate a finite region of contact, the size of which will depend on material properties and contact forces. The contact mechanics will also determine the level of penetration or relative closure of the TDB and rotor geometric centres under contact. In the limiting case of zero penetration, or infinite contact stiffness, dynamic contact forces become idealized impulsive approximations to the practically finite contact forces. We also remark that considerable uncertainty of contact conditions may arise from angular misalignment between a rotor and TDB. The impulsive approximation therefore provides an impact model, against which consistent rotor dynamic behaviour may be derived. For this reason, it is adopted in this paper. Predicted rotor motions will then generally involve sequences of instantaneous impacts determined by impulsive normal and tangential forces [22].

The nature of impacts, which involves an impulsive collision with rebound and the simultaneous action of Coulomb friction, is a rich area of study as a number of different scenarios may occur at the collision depending upon the relative normal and tangential velocities [12,19]. Indeed in [12] a series of different impact models are presented for various different cases, with special subtlety occurring when the relative tangential velocity changes sign during the collision. However, in the case of the problem we are considering, two aspects of the model simplify the choice of collision model. Firstly, we assume that the TDB is perfectly circular and with a larger radius ($R + c_r$) than that of the rotor (R). Secondly, the fact that the rotor is spinning very fast and with high energy, means that the relative tangential velocity is high and (as we will show) does *not* come close to changing sign during impact. Thus, all impacts can be modelled using *Case 1* of the models described in [12].

To model such impacts, i.e. if the rotor centre $|z| = c_r$, we assume that the system experiences the ith instantaneous collision at time τ_i with $i \in \{0, 1, 2, \ldots\}$, and in that case a *reset law* applies, which changes the velocity of the centre of the rotor. By $\tau_{i,-}$ we denote the time *immediately before* the impact and by $\tau_{i,+}$ the time *immediately after* the impact. Before stating the reset law, we specify our assumptions about the nature of this collision. Firstly, the TDB is assumed to be infinitely stiff and to behave like a fixed impact surface. In this limiting case of zero penetration, or infinite contact stiffness, dynamic contact forces become idealized impulsive approximations to the practically finite contact forces. Secondly, as the rotational speed $\Omega > 0$ of the rotor is high, the change of Ω during impact is negligible. Hence we presume that it remains unchanged during impact and that the effect of the impact is to only alter the radial and angular velocity of the centre of the rotor. In particular, we assume that *immediately before* the impact at $\tau_{i,-}$ these velocities take the values $\dot{\tilde{r}}_{i,-}$, $\dot{\tilde{\theta}}_{i,-}$ and values $\dot{\tilde{r}}_{i,+}$, $\dot{\tilde{\theta}}_{i,+}$ *immediately after* at $\tau_{i,+}$. Thirdly, at the point of contact CP (figure 1), the relative tangential velocity $v_{\mathrm{rel},i,\pm}$ between the rotor and TDB immediately before and after the impact is given by

$$v_{\mathrm{rel},i,\pm} = R\Omega + c_r\dot{\tilde{\theta}}_{i,\pm}. \tag{2.3}$$

In §4 (4.11), and also more generally at the end of §5, we will estimate the value of $\dot{\tilde{\theta}}_{i,-}$. Significantly, for the examples considered, both Ω and the ratio R/c_r are *large* and as a

consequence, for the moderately sized values of $\dot{\tilde{\theta}}$ and $\dot{\tilde{r}}$ computed, we have that

$$\dot{\tilde{\theta}}_{i,\pm} > \frac{-R\Omega}{c_r}. \tag{2.4}$$

It follows that the relative tangential velocity both before and after the impact is positive. As a result, we may use the impact law described as *Case 1* in [12] and that the three coefficient of restitution models, i.e. kinetic, kinematic and energetic, yield the same impact velocity, [12,19]. By contrast, it has been shown in [19] that if $v_{\mathrm{rel},i,-}$ is not constant during an instantaneous impact with friction, then the kinetic and kinematic models can lead to a non-physical increase in kinetic energy.

At the impact time $\tau_{i,-}$ the rotor experiences BOTH an impulsive normal contact force F_c in the normal-(z) direction and an associated impulsive frictional force F_f in the tangential (iz)-direction. The energy dissipation in the normal contact direction is approximated by Newton's coefficient of restitution d and in the tangential contact direction by Coulomb's coefficient of friction μ. This gives

$$F_c = -(1+d)\dot{\tilde{r}}_{i,-}\delta(\tau - \tau_{i,-}) \tag{2.5}$$

and (using the condition (2.4))

$$F_f = -\mu\ \mathrm{sgn}(v_{\mathrm{rel},i,-})F_c = -\mu F_c = -\mu(1+d)m\dot{\tilde{r}}_{i,-}\delta(\tau - \tau_{i,-})$$

where sgn is the sign function, $\dot{\tilde{r}}_{i,-} > 0$ is the radial impact velocity and δ is the Dirac delta function. Under these assumptions, the position of the rotor centre z is unchanged by the impact so that

$$z(\tau_{i,+}) = z(\tau_{i,-}) =: z_i. \tag{2.6}$$

By contrast, at the contact point, CP the rotor's radial and angular velocities change instantaneously and we have

$$\dot{\tilde{r}}_{i,+} = -d\dot{\tilde{r}}_{i,-}, \tag{2.7}$$

$$R\Omega + c_r\dot{\tilde{\theta}}_{i,+} = R\Omega + c_r\dot{\tilde{\theta}}_{i,-} - \mu(1+d)\dot{\tilde{r}}_{i,-},$$

so that

$$\dot{\tilde{\theta}}_{i,+} = \dot{\tilde{\theta}}_{i,-} - \mu(1+d)\frac{\dot{\tilde{r}}_{i,-}}{c_r}. \tag{2.8}$$

Again, we note that as $\Omega \gg 1$ and also $R/c_r \gg 1$, that for the examples computed in §4, the relative tangential velocity $v_{\mathrm{rel},i,\pm}$, given by (2.3), is positive, which is the consistency condition for the use of this impact law as described in [12]. More detail on this condition will be given in §4.

While this reset law is linear, the equations of motion between impacts are nonlinear in this coordinate frame $(\tilde{r},\tilde{\theta})$, and it is more convenient for further analysis to use the complex coordinates, in which the equations of motion are linear. In the $(\tilde{x},\tilde{y})$ Cartesian frame with $z = \tilde{x} + i\tilde{y}$ the reset law (2.7) and (2.8) corresponds to the nonlinear expression

$$\dot{z}(\tau_{i,+}) = \dot{z}(\tau_{i,-}) - q\frac{\mathrm{Re}(z_i^*\dot{z}(\tau_{i,-}))z_i}{|z_i|^2} = \dot{z}(\tau_{i,-}) - q\,\dot{\tilde{r}}_{i,-}\frac{z_i}{|z_i|}, \tag{2.9}$$

where $q = (1+d)(1+\mathrm{i}\mu)$, z_i^* is the complex conjugate of z_i and $\dot{\tilde{r}}_{i,-} = \mathrm{Re}(z_i^*\dot{z}(\tau_{i,-}))/|z_i|$.

It is convenient for further computations to introduce a co-rotating frame with complex coordinate u so that

$$u = z\,\mathrm{e}^{-\mathrm{i}\Omega\tau} \equiv \tilde{r}\,\mathrm{e}^{\mathrm{i}(\tilde{\theta}-\Omega\tau)}.$$

As the name indicates, this frame rotates synchronously with the rotor at speed Ω. This will be advantageous when examining limit cycles, which impact synchronously with the rotor's rotation. Furthermore, we non-dimensionalize the system both to reduce the number of free

parameters and also to show that no natural large or small parameters are present in this system. We introduce a scaled time t

$$t = \Omega\tau, \quad \text{so that } \frac{\mathrm{d}}{\mathrm{d}\tau} = \Omega\frac{\mathrm{d}}{\mathrm{d}t} \quad \text{and} \quad \delta(\tau - \tau_{i,-}) = \Omega\delta(t - t_{i,-}). \tag{2.10}$$

This new term moves through one period in time $t = 2\pi$ if the original time goes through one period of the forcing term, $2\pi/\Omega$. In the fixed frame, we introduce the dimensionless polar coordinates (r, Θ) and the complex coordinate Z,

$$r = \frac{\tilde{r}}{c_\mathrm{r}}, \quad \Theta = \tilde{\theta} \quad \text{and} \quad Z \equiv r\,\mathrm{e}^{\mathrm{i}\Theta} = \frac{z}{c_\mathrm{r}}$$

which, in the co-rotating frame, correspond to the polar coordinates (r, θ) and the complex coordinate U given by

$$\theta \equiv \Theta - t = \tilde{\theta} - \Omega\tau \quad \text{and} \quad U \equiv r\,\mathrm{e}^{\mathrm{i}\theta} = \frac{u}{c_\mathrm{r}}. \tag{2.11}$$

The motion of the rotor is considered to be in a forward sense if $\dot{\tilde{\theta}}(\tau) > 0$, i.e. in scaled coordinates $\dot{\Theta}(t) > 0$ or $\dot{\theta}(t) > -1$, in a backward sense if $\dot{\tilde{\theta}}(\tau) < 0$, i.e. in scaled coordinates $\dot{\Theta}(t) < 0$ or $\dot{\theta}(t) < -1$, and synchronous if $\dot{\tilde{\theta}}(\tau) = \Omega$, corresponding to scaled coordinates $\dot{\Theta}(t) = 1$ or $\dot{\theta}(t) = 0$. We define the dimensionless parameters

$$\gamma = \frac{c}{m\Omega}, \quad \omega^2 = \frac{k}{m\Omega^2} \quad \text{and} \quad \rho = \frac{e_c}{c_\mathrm{r}}. \tag{2.12}$$

Substituting (2.10)–(2.12) into (2.2), cancelling the factor of $\mathrm{e}^{\mathrm{i}\Omega\tau}$ and dividing by $m\Omega^2$ then the equation of motion (2.2) in the scaled co-rotating complex coordinate U becomes

$$\ddot{U} + (\gamma + 2i)\dot{U} + (\omega^2 - 1 + i\gamma)U = \rho\,\mathrm{e}^{\mathrm{i}\phi} \quad \text{if } |U| \le 1, \tag{2.13}$$

where dots now refer to differentiation with respect to t. In the scaled coordinates, an impact occurs if $|U| \equiv r = 1$. Consequently, the reset law (2.6), (2.9) in the scaled coordinates is

$$U(t_{i,+}) = U(t_{i,-}) \equiv U(t_i), \tag{2.14}$$

$$\dot{U}(t_{i,+}) = \dot{U}(t_{i,-}) - q\dot{r}(t_{i,-})U(t_i), \tag{2.15}$$

where $\dot{r}(t_{i,-}) = \mathrm{Re}(U^*(t_i)\dot{U}(t_{i,-}))$. The choices of parameters (in consistent units) corresponding to the experimental application in [22] are

$$m = 50\,\mathrm{kg}, \quad c = 1400\,\mathrm{N\,s\,m^{-1}}, \quad k = 9.8 \times 10^5\,\mathrm{N\,m^{-1}}, \quad e_c = 0.3 \times 10^{-3}\,\mathrm{m},$$
$$c_\mathrm{r} = 0.7 \times 10^{-3}\,\mathrm{m}, \quad R = 0.4 \times 10^{-1}\,\mathrm{m}, \quad \phi = 0.21\,\mathrm{rad}, \quad \Omega = 184.2\,\mathrm{rad\,s^{-1}},$$
$$\mu = 0.15, \quad d = 0.95,$$

and the dimensionless parameters are

$$\gamma \approx 0.152, \quad \omega \approx 0.76, \quad \rho = \frac{3}{7} \approx 0.428, \quad \phi = 0.21\,\mathrm{rad}, \quad \mu = 0.15,$$
$$d = 0.95, \quad \frac{R}{c_\mathrm{r}} = 57.143.$$

In this paper, the coefficient $\gamma > 0$ (associated with damping) will act as the bifurcation parameter and the remaining parameters will take the values given above.

3. Basic solution dynamics and associated maps

In this section, we introduce the simplest basic solution types in the co-rotating frame, and in particular study solutions, which are either not in contact, or could lead to continuous contact, or

have instantaneous impacts. To analyse the system described in §2, we consider those piecewise-smooth orbits, which comprise smooth trajectories interrupted by impulsive collisions. Such orbits are not uncommon in the motions of mechanical systems with constraints and can be studied using a variety of different methods. One such is the method of measure differential inclusions described in §1 [3–7], in which the ODEs describing the system have measure valued right-hand sides, which include the impulsive terms used to describe the effects of the impacts. Such methods are effective for deriving results about complex motions in such problems. As an alternative, we can use the method of recasting the magnetic bearing problem as a hybrid system [8–13], in which we consider flows alternating with maps when a certain constraint on the orbit is realized. The relative simplicity of the flow equations in (2.13) and of the reset law (2.14), (2.15), allow a direct implementation of this method, which is particularly suitable for studying the existence, stability and bifurcations of the single impact periodic orbits we consider in this paper.

(a) Maps and flows

To calculate the flows, we rewrite the scaled equations of motion (2.13) as a first-order complex dynamical system. This will be helpful in the global and local analysis of a periodically impacting orbit presented in later sections. Let the complex vector

$$\boldsymbol{w}(t) = (U(t), \dot{U}(t))^{\mathrm{T}},$$

then in free flight the system satisfies the ordinary differential equation

$$\dot{\boldsymbol{w}}(t) = A\boldsymbol{w}(t) + \boldsymbol{b}, \quad \text{if } |U| \le 1 \tag{3.1}$$

where the matrix A and the vector $\boldsymbol{b}$ are constant and are defined by

$$A = \begin{pmatrix} 0 & 1 \\ 1-\omega^2 - \mathrm{i}\gamma & -\gamma - 2\mathrm{i} \end{pmatrix} \quad \text{and} \quad \boldsymbol{b} = \begin{pmatrix} 0 \\ \rho\, \mathrm{e}^{\mathrm{i}\phi} \end{pmatrix}. \tag{3.2}$$

Assume an impact occurs, i.e. $|U| = 1$, at time t_i. The set of the states $\boldsymbol{w}$ at impact is referred to as the impact surface $\Sigma = \{\boldsymbol{w} : |U| = 1\}$. It follows from (2.14), (2.15) that the reset law R, mapping $\boldsymbol{w}_{i,-}$ to $\boldsymbol{w}_{i,+}$, takes the form

$$\boldsymbol{w}(t_{i,+}) = R(\boldsymbol{w}(t_{i,-})) \equiv \boldsymbol{w}(t_{i,-}) - \begin{pmatrix} 0 \\ q\dot{r}_{i,-}U(t_i) \end{pmatrix}. \tag{3.3}$$

For convenience, we introduce the simplified notation $\boldsymbol{w}(t_{i,\pm}) =: \boldsymbol{w}_{i,\pm}$.

As the flow equation (3.1) is linear and the vector $\boldsymbol{b}$ is a constant the general solution with initial conditions $\boldsymbol{w}_{i,+}$ can be written as

$$\boldsymbol{w}(t) = S(t - t_{i,+}, \boldsymbol{w}_{i,+}) \equiv \exp(A(t - t_{i,+}))(\boldsymbol{w}_{i,+} + A^{-1}\boldsymbol{b}) - A^{-1}\boldsymbol{b}, \quad \text{if } |U| \le 1. \tag{3.4}$$

The eigenvalues $\lambda_\pm$ of the matrix A are given by

$$\lambda_\pm = \frac{-\gamma + \mathrm{i}\left(-2 \pm \sqrt{4\omega^2 - \gamma^2}\right)}{2} \tag{3.5}$$

with real part $\mathrm{Re}(\lambda_\pm) = -\gamma/2 < 0$, as we assume (given the experimentally defined values) that $0 < \gamma < 2\omega$. It is immediate from this calculation that the trajectories of the magnetic bearing system between impacts depend smoothly upon the initial data in an explicitly calculable manner.

A systematic approach to studying the impacting dynamics of the magnetic bearing problem is to consider the associated map relating one impact event to the next. To do this, consider an orbit with state vector immediately before an impact at time $t_{i,-}$ given by $\boldsymbol{w}_{i,-}$ with $|U_i| = 1$ and $\dot{r}_{i,-} > 0$. At the point of impact, we may now apply the reset law R in (3.3) to give the new state vector $\boldsymbol{w}_{i,+}$ immediately after the impact at time $t_{i,+}$. As $\dot{r}_{i,+} < 0$, such initial conditions lead to a trajectory described by the flow map S, initially lying inside the TDB. After a first time interval $t \in (t_i, t_{i+1})$ with the period $T = t_{i+1} - t_i > 0$ (which may possibly be infinite), the orbit will impact

again with the TDB at time t_{i+1} when $|U_{i+1}|=1$. Provided that $r_{i+1,-}>0$ (a non-grazing or a transversal intersection), then T itself depends in a smooth manner upon the initial data [10], but it is, in general, a nonlinear function of these, which cannot be calculated explicitly. The impact map $P_{\mathrm{I}}:\Sigma\to\Sigma$ is then defined by

$$\boldsymbol{w}_{i+1,-}=P_{\mathrm{I}}(\boldsymbol{w}_{i,-})\equiv S(t_{i+1}-t_i,R(\boldsymbol{w}_{i,-})).$$

This map is uniquely defined provided that $\dot{r}_{i,-}>0$ and is smooth provided that $\dot{r}_{i+1,-}>0$ [10]. The cases, for which $\dot{r}_{i+1}=0$ are grazing events, and mark dramatic changes in the stability of the system, which we will not be considering in this paper. The advantage of this construction is that we can reduce the dimension of the problem by one as the radial coordinate $r\equiv|U|=1$ at impact. We note that this is just one of many maps, which can describe the system. An alternative is the stroboscopic map [10], which samples the system at the periodic time intervals and must be augmented, typically through additional saltation matrices, to allow for the effects of impacts. Such maps are useful in understanding the dynamics when the system involves grazing.

The dynamics of the rotor, experiencing impacts, can now be described in general, in terms of successive iterates of the map P_{I}. We now highlight the different possible motions of the rotor.

(b) Equilibria

In the *absence* of impacts it follows immediately from (3.1), and the negative real part of the eigenvalues of A, that there is an asymptotically stable equilibrium solution $\boldsymbol{w}=\boldsymbol{w}^*$ of the flow equation (3.1), which satisfies the condition

$$\dot{r}=\dot{\theta}=0. \tag{3.6}$$

This is given by

$$\boldsymbol{w}^*\equiv(U^*,\dot{U}^*)^{\mathrm{T}}=-A^{-1}\boldsymbol{b}=\left(\frac{\rho\,\mathrm{e}^{\mathrm{i}\phi}}{\omega^2-1+\mathrm{i}\gamma},0\right)^{\mathrm{T}}. \tag{3.7}$$

Let $\gamma^*=\sqrt{\rho^2-(1-\omega^2)^2}$. Depending on the bifurcation parameter γ this equilibrium can lie either

(i) inside the TDB ($r\equiv|U|<1$), if $\gamma>\gamma^*$. This equilibrium, $\boldsymbol{w}=\boldsymbol{w}^*=:\boldsymbol{w}^*_{\mathrm{r}}$, is physically realistic; we denote this steady state as *admissible*,
(ii) on the TDB ($r=1$), if $\gamma=\gamma^*$. The point $\boldsymbol{w}=\boldsymbol{w}^*=:\boldsymbol{w}^*_{\mathrm{B}}$, $\gamma=\gamma^*$ is referred to as a *boundary equilibrium* point or
(iii) outside the TDB ($r>1$), if $\gamma<\gamma^*$. This equilibrium is physically unrealistic, and we denote this steady state as *virtual*.

By extension, this nomenclature is implemented for other orbits, so that a periodic orbit is virtual, if it wholly or in part lies outside of the TDB. In Case (i), the motion is called synchronous non-contacting whirl (figure 2*a*). Case (ii) describes the critical transition point between physically realistic (Case (i)) and physically unrealistic non-impacting equilibria (Case (iii)). At a boundary equilibrium point, the admissible equilibrium may bifurcate into more complicated rotor trajectories, such as those involving continuous (zero normal velocity and non-negative normal acceleration) or instantaneous rotor-TDB contact. Then this point is referred to as a BEB. When the rotor and TDB are in continuous contact, sliding or pure rolling are possible [22]. The tangential slip velocity between the rotor and TDB may be extended from (2.3) to cover continuous contact using $v_{\mathrm{rel}}(\tau)=R\Omega+c_{\mathrm{r}}\dot{\tilde{\theta}}(\tau)$. Forward whirl rotor orbits correspond with $\dot{\tilde{\theta}}(\tau)>0$ and backward whirl orbits with $\dot{\tilde{\theta}}(\tau)<0$. In terms of the scaled polar coordinate in the co-rotating frame, these orbits correspond with $\dot{\theta}(t)>-1$ and $\dot{\theta}(t)<-1$, respectively. Synchronous forward whirl occurs when $\dot{\theta}(t)=0$, which is the condition for the equilibrium given in (3.6), in which case the tangential slip velocity $v_{\mathrm{rel}}(\tau)=(R+c_{\mathrm{r}})\Omega$ is *always positive*. The slip velocity only changes sign

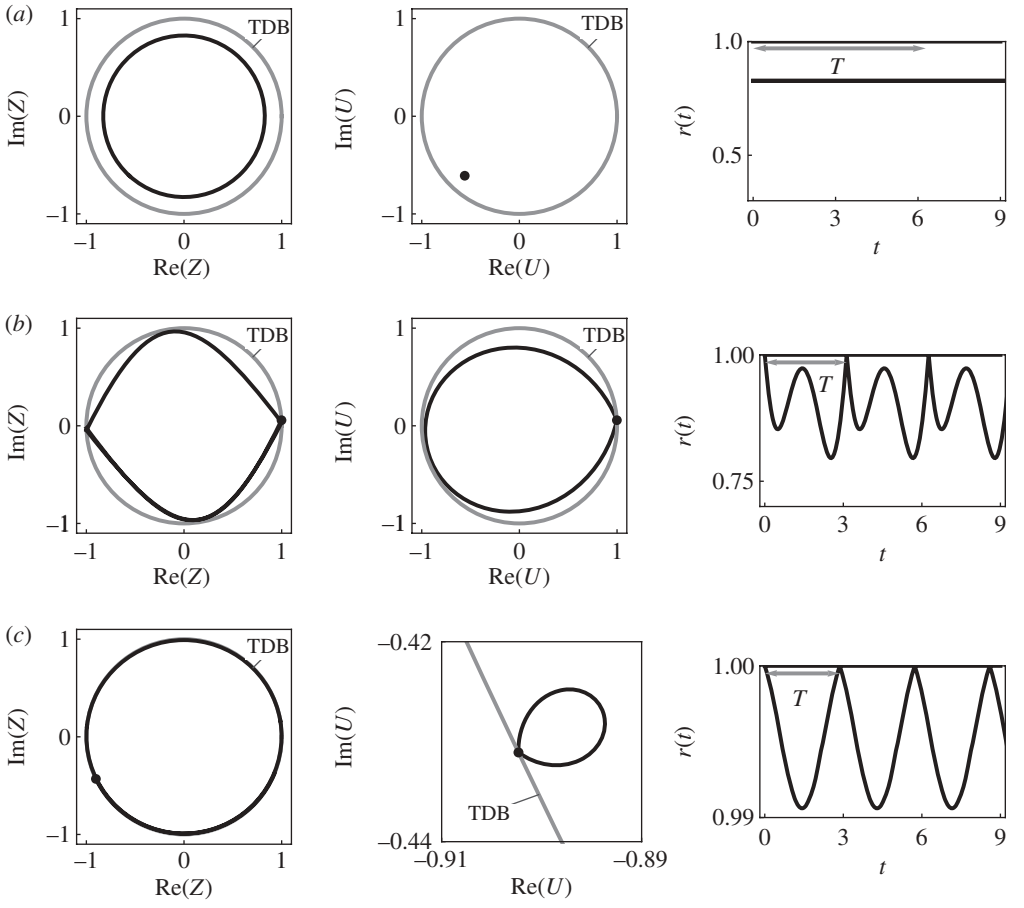

Figure 2. Orbits with period T in the inertial frame (Z), the co-rotating frame (U), and where $r(t)$ is against time t. An impact occurs if $r \equiv |Z| \equiv |U| = 1$. (*a*) Admissible equilibrium without impact ($\gamma = 0.3$). (*b*) Impacting limit cycle $B_{1,d}$ near grazing ($\gamma = 0.065$). (*c*) Impacting limit cycle $B_{1,a}$ near NSH bifurcation, ($\gamma = 0.1$).

when $\dot{\tilde{\theta}}(\tau) = -R\Omega/c_r$, which corresponds to pure rolling with $\dot{\theta}(t) = -(R + c_r)/c_r$. The implication of this is that the contact friction will have the same tangential sense in opposing the rotation for most rub conditions, apart from those in which the backward orbit angular velocity is less than $\dot{\theta}(t) = -(R + c_r)/c_r$. In practice, forward rubs are relatively common events, while the backward whirl conditions involving pure rolling are infrequent and tend to coincide with mechanical failure due to the high contact forces that coexist. For this reason, we consider only synchronous forward whirl rubbing. Continuous contact motions are not studied in this paper as the reset law is not sufficient to describe such behaviour and how it arises, but more detail is given in [42].

(c) Periodic orbits with impact

We will consider periodic impacting motions of the rotor and their bifurcations from boundary equilibrium states. When the rotor experiences an instantaneous contact with the TDB it can lead to orbits that impact periodically or quasi-periodically and synchronously in the co-rotating frame (figure 2*b*,*c*). We call these *period T synchronously impacting limit cycles* as the orbit experiences one impact per period T. Such orbits have been observed in numerical experiments reported in [22], where they are found to either be globally attracting or to have large basins of attraction. As we shall see in §4, limit cycles with small amplitude (as shown in figure 2*c*) are created in an NSH-type bifurcation from a boundary equilibrium as parameters in the system vary. Limit cycles with

large amplitude (figure 2*b*) can also exist, and these can both experience smooth bifurcations (fold, period-doubling, homoclinic, etc.) or can change at (discontinuity-induced) grazing bifurcations [11], when the trajectory interacts tangentially with the boundary of the bearing.

A systematic way of analysing such periodic motions with instantaneous impact, is to consider them as periodic orbits of the map P_{I}. Such an approach is very suitable for finding both the existence and the stability of periodic orbits [10] and we will adopt it here. In this framework, single impact orbits are simply fixed points of P_{I} so that

$$\boldsymbol{w}_{i+1,-} = P_{\mathrm{I}}(\boldsymbol{w}_{i,-}) = \boldsymbol{w}_{i,-}. \tag{3.8}$$

Given the known form of both the flow map S between impacts and the reset law R, the condition (3.8) leads to a system of algebraic equations, which includes finding the time of flight T. We will consider this system in §4, and its linearization, in §5.

(d) Other dynamics

In addition to periodic [21,42] or quasi-periodic orbits [20,42], it has been shown that in similar models the rotor–stator interaction can be chaotic [20,42]. Other types of motion can include an accumulation of an infinite number of impacts (with the impact velocity decreasing in a geometric progression), in a finite time [20,42,43]. This behaviour, which arises when the rotor is being forced towards the TDB at the same time as it rebounds from it, is often called *chattering* [44–46] in the context of impact dynamics. Chattering can lead to sticking [46] and sliding motion [10] and hence can be used to predict the onset of continuous contact motion without actually computing continuous contact trajectories. It is closely related to the Zeno-type accumulation behaviour found in hybrid systems [8] but differs from chattering in discontinuous control problems, where an orbit repeatedly crosses the surface across which the control system is discontinuous [47]. Li & Païdoussis [20] have used this behaviour to identify for what values of coefficient of friction, μ, and eccentricity, e_c, continuous contact motion occurs. Similarly, the occurrence of chattering sequences and the possibly resulting continuous contact also depends on damping, c, and stiffness, k, parameters [42]. Such, particle motion involving continuous contact over an open time interval, can best be systematically described by set valued functions instead of hybrid systems. These types of models, called *differential inclusion* are particularly well suited to analyse problems involving only friction, e.g. sliding and sticking motion of rotating particles [48]. Such a model, a forced rotating pendulum in continuous contact with a circular boundary, shows similar features to ours in that various orbits collapse onto the equilibrium set in finite time [49]. While it is certainly possible that such chattering and sticking motions may arise in a magnetic bearing system, in this paper we will restrict our analysis to that of the simpler types of periodic motion described.

4. Global analysis of synchronously impacting limit cycles

In this section, we derive the existence conditions for the simplest type of limit cycles for the full system, in which the periodic orbits have one instantaneous impact synchronous with the co-rotating frame. These are supported by numerical calculations. We show that these invariant sets undergo both smooth fold bifurcations and discontinuity-induced NSH-like bifurcations, where they are created in pairs at a BEB simultaneously with the admissible equilibrium $\boldsymbol{w} = \boldsymbol{w}_R^*$. In §5, we give a local analysis of the latter bifurcation in a more general setting. We also discuss the stability of these limit cycles in §4*a* and the codimension-2 bifurcations related to the Hopf-type bifurcation (with dependence on the scaled stiffness parameter ω) in §4*b*. These, period T periodically impacting limit cycles, experience one impact per cycle with identical impact velocity $\dot{U}(t_{i,-})$ at each impact event at time t_i for $i = 0, 1, 2 \ldots$. We further assume that these impacts occur synchronously with respect to the co-rotating frame. As a consequence, the impact position $U(t_i)$ is identical at each impact at time t_i and satisfies the repeatable initial conditions between consecutive impacts at time t_i and t_{i+1} given by condition (3.8). It follows

that, in polar coordinates, the radial and angular velocity components must satisfy $\dot{r}_{i,-} = \dot{r}_{i+1,-}$ and $\dot{\theta}_{i,-} = \dot{\theta}_{i+1,-}$. We will show that for certain values of the scaled damping parameter, γ, a finite number of such limit cycles coexist with the admissible equilibrium $\boldsymbol{w} = \boldsymbol{w}_R^*$. We will then demonstrate that only one set of a pair of physically plausible limit cycles with different period T undergoes a DIB at the BEB point when $\gamma = \gamma^* =: \gamma_{\mathrm{DIB}}$. That bifurcation will be shown to be of *NSH* type, as two limit cycles collide with the boundary equilibrium point $\boldsymbol{w} = \boldsymbol{w}_B^*$, as their amplitude shrinks to zero. We conclude §4 with determining for which parameter value, γ, these limit cycles are admissible and stable.

To find fixed points, $\boldsymbol{w}_{0,-}$ satisfying (3.8), we substitute the initial condition $\boldsymbol{w}_{0,+}$ into the general solution of the flow given by (3.4) to obtain

$$\boldsymbol{w}_{0,-} = \exp(AT)(\boldsymbol{w}_{0,+} + A^{-1}\boldsymbol{b}) - A^{-1}\boldsymbol{b},$$

where A and $\boldsymbol{b}$ are given in (3.2), and where the real part of the eigenvalues of A, given in (3.5), is negative, i.e. $\mathrm{Re}(\lambda_\pm) = -\gamma/2 < 0$ for $\gamma > 0$. Next, we apply the reset map and substitute $\boldsymbol{w}_{0,+} = R(\boldsymbol{w}_{0,-})$ from (3.3) to obtain, after some manipulation, the fixed point equation

$$\boldsymbol{w}_{0,-} = -(\exp(-AT) - I)^{-1} \begin{pmatrix} 0 \\ q\dot{r}_{0,-}U_0 \end{pmatrix} - A^{-1}\boldsymbol{b}. \tag{4.1}$$

The matrix expression can be simplified further by considering the eigendecomposition of $A = VDV^{-1}$. Then

$$\begin{aligned}(\exp(-AT) - I)^{-1} &= \frac{1}{1 - \mathrm{tr}(\exp(AT)) + \det(\exp(AT))}(\exp(AT) - \det(\exp(AT))I) \\ &= \frac{1}{1 - \mathrm{tr}(\exp(DT)) + \exp(\mathrm{tr}(AT))}(\exp(AT) - \exp(\mathrm{tr}(AT))I)\end{aligned}$$

by Jacobi's formula. Finally, we can use the eigenvalues of A, λ_+ and λ_-, given in (3.5), to obtain

$$\begin{aligned}(\exp(-AT) - I)^{-1} &= \kappa \begin{pmatrix} \nu_- e^{\lambda_+ T} - \nu_+ e^{\lambda_- T} - e^{\Lambda T} & \nu_+\nu_-(e^{\lambda_- T} - e^{\lambda_+ T}) \\ e^{\lambda_+ T} - e^{\lambda_- T} & \nu_- e^{\lambda_- T} - \nu_+ e^{\lambda_+ T} - e^{\Lambda T} \end{pmatrix} \\ &=: \begin{pmatrix} a_{11}(T) & a_{12}(T) \\ a_{21}(T) & a_{22}(T) \end{pmatrix},\end{aligned}$$

where $\Lambda = \lambda_+ + \lambda_-$, $\nu_\pm = -\lambda_\pm/(1 - \omega^2 - \mathrm{i}\gamma)$ and $\kappa = 1/((1 - e^{\lambda_- T})(1 - \mathrm{e}^{\lambda_+ T})(\nu_- - \nu_+))$. Hence substituting this matrix into (4.1) simplifies to

$$\boldsymbol{w}_{0,-} \equiv \begin{pmatrix} U_0 \\ \dot{U}_{0,-} \end{pmatrix} \equiv \begin{pmatrix} \mathrm{e}^{\mathrm{i}\theta_0} \\ \dot{r}_{0,-} + \mathrm{i}\dot{\theta}_{0,-})U_0 \end{pmatrix} = \begin{pmatrix} -qa_{12}(T)\dot{r}_{0,-}U_0 + K \\ -qa_{22}(T)\dot{r}_{0,-}U_0 \end{pmatrix}, \tag{4.2}$$

where $K = \rho\,\mathrm{e}^{\mathrm{i}\phi}/(\omega^2 - 1 + i\gamma)$. The system (4.2) yields three equations by solving the first row equation for U_0, taking the real part of the second row equation and solving it for $\dot{r}_{0,-}$, and taking the imaginary part of the second row equation, respectively,

$$U_0(1 + a_{12}(T)q\dot{r}_{0,-}) = K, \tag{4.3}$$

$$\dot{r}_{0,-}(1 + \mathrm{Re}(qa_{22}(T))) = 0 \tag{4.4}$$

and

$$\dot{\theta}_{0,-} = -\,\mathrm{Im}(qa_{22}(T))\dot{r}_{0,-}. \tag{4.5}$$

To determine the fixed points $\boldsymbol{w}_{0,-}$ from (4.2), we first find the period T, unknown a priori, from (4.4) and then compute the corresponding values $\dot{r}_{0,-}$ from (4.3), θ_0 from (4.3) and $\dot{\theta}_{0,-}$ from (4.5). Now, (4.4) is satisfied if $\dot{r}_{0,-}$ is zero, which only yields the boundary equilibrium $\boldsymbol{w}_B^*$, or if the nonlinear term in T, denote it by $F_1(T)$, is zero. Hence the period T can be determined by finding

the zeros of $F_1(T)$, given by

$$F_1(T) := 1 + \mathrm{Re}(qa_{22}(T)) = 1 - \mathrm{Re}\left(\frac{q}{\lambda_+ - \lambda_-}\left(\frac{\lambda_+ e^{\lambda_+ T}}{e^{\lambda_+ T} - 1} - \frac{\lambda_- e^{\lambda_- T}}{e^{\lambda_- T} - 1}\right)\right)$$
$$= 1 + \frac{\tilde{d}e^{-\gamma T/2}}{2s_1}\left(\frac{s_2^- e^{\gamma T/2} - 2s_3^- e^{\gamma T}\cos(s_4^- T + \zeta^-)}{1 + e^{\gamma T} - 2e^{\gamma T/2}\cos(s_4^- T)} + \frac{-s_2^+ e^{\gamma T/2} + 2s_3^+ e^{\gamma T}\cos(s_4^+ T + \zeta^+)}{1 + e^{\gamma T} - 2e^{\gamma T/2}\cos(s_4^+ T)}\right), \tag{4.6}$$

where $\tilde{d} = 1 + d$, $s_1 = \sqrt{4\omega^2 - \gamma^2}$, $s_2^{\mp} = 2 \mp s_1 + \gamma\mu$, $s_3^{\mp} = \sqrt{(1+\mu^2)(1+\omega^2 \mp s_1)}$, $s_4^{\mp} = (\mp 2 + s_1)T/2$, $s_5^{\mp} = \pm\gamma + (\mp 2 + s_1)\mu$ and $\zeta^{\mp} = 2\arctan(s_5^{\mp}/(s_3^{\mp} + s_2^{\mp}))$.

We now consider the analytic form of $F_1(T)$. It is evident from (4.6) that it is oscillatory in T. If $\gamma > 0$ then the oscillations have decreasing amplitude as the period T increases and $F_1(T)$ tends to one as T tends to infinity. If T is fixed and $\gamma > 0$ increases, then the amplitude of the oscillations also decreases to zero. Furthermore, if we fix γ and assume that T is large, then

$$F_1(T) \approx 1 + \frac{(1+d)\,\mathrm{e}^{-\gamma T/2}}{s_1}(-s_3^- \cos(s_4^- T + \zeta^-) + s_3^+ \cos(s_4^+ T + \zeta^+)) \tag{4.7}$$

and is bounded, i.e. $F_1^-(T) < F_1(T) < F_1^+(T)$, where

$$F_1^{\pm}(T) = 1 \pm \frac{(1+d)\,\mathrm{e}^{-\gamma T/2}}{s_1}(s_3^- + s_3^+). \tag{4.8}$$

The upper and lower bounds $F_1^{\pm}(T)$ are positive for all large T. Therefore, for fixed parameters, and if $\gamma > 0$ the nonlinear function $F_1(T)$ has finitely many zeros. This is consistent with the plots presented in figure 3*a*. As γ decreases and the amplitude of the oscillations of F_1 increase then more zeros arise pairwise. Moreover, if γ is zero then $F_1(T)$ is purely oscillatory and hence has infinitely many zeros. The period T depends on the damping parameter, γ, the stiffness, ω, the coefficient of restitution, d and the coefficient of friction, μ. Therefore varying the scaled unbalance radius ρ, or unbalance angle ϕ will not affect it. We illustrate the period's dependence on γ in a bifurcation plot for fixed parameters $\omega = 0.76$, $d = 0.95$ and $\mu = 0.15$ (figure 3*a*). This figure not only illustrates the existence of a finite number of zeros for $\gamma \in (0, \gamma_{F,1} \approx 0.178)$ and hence of fixed points of the map P_1 of a period T, but also shows that no such fixed points exist otherwise. The next variable, normal impact velocity, $\dot{r}_{0,-}$, can now be determined from T by taking the absolute value of (4.3) and solving for $\dot{r}_{0,-}$. Then for each value of the period T, $\dot{r}_{0,-}$ has two solutions $\dot{r}_{0,-,a}$ and $\dot{r}_{0,-,c}$ given by

$$\dot{r}_{0,-,c/a}(T) = \frac{-g(T) \pm \sqrt{g(T)^2 - |q|^2|a_{12}(T)|^2(1 - |K|^2)}}{|q|^2|a_{12}(T)|^2}, \tag{4.9}$$

where $g(T) = (1+d)(\mathrm{Re}(a_{12}(T)) - \mu\ \mathrm{Im}(a_{12}(T)))$. However, we observe that these solutions may themselves coalesce at a fixed bifurcation at $\gamma = \gamma_F^- \approx -0.497$ (figure 4*a*). But as γ_F^- is negative it has no physical context on the application. As γ is increased these two branches persist under varying stability and admissibility. A fixed point is potentially *admissible* if the rotor is approaching the impact surface from within the clearance circle, i.e. $\dot{r}_{0,-} > 0$. Otherwise ($\dot{r}_{0,-} < 0$), it is *virtual*. Note that one of the radial velocities (4.9) becomes zero if $1 - |K|^2 = 0$, i.e. when $\gamma = \gamma^*$. From figure 4, it is evident that only low radial impact velocity fixed points undergo a sign change in $\dot{r}_{0,-}$. The angle at impact θ_0 and the angular impact velocity $\dot{\theta}_{0,-}$, do not need any constraints imposed upon them to ensure admissibility. From (4.3) and (4.5), we obtain their expressions, respectively,

$$\theta_0(T, \dot{r}_{0,-}) = \mathrm{Arg}\left(\frac{K}{1 + a_{12}(T)q\dot{r}_{0,-}}\right) \tag{4.10}$$

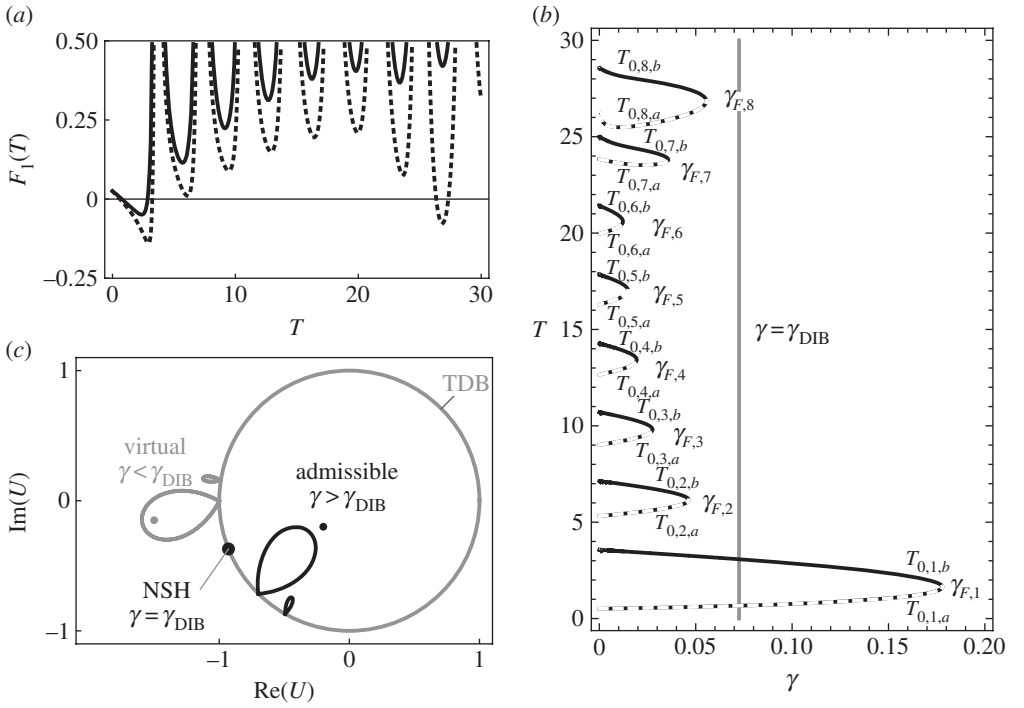

Figure 3. (*a*) The function $F_1(T)$ against T with $\gamma = 0.1$ (black) and with $\gamma = 0.05$ (dashed). (*b*) The zeros $T_{0,n,m}$ of F_1 as the damping coefficient γ is varied with branches $T_{0,n,a}$ (dashed) and $T_{0,n,b}$ (solid), ($\gamma_{F,1} \approx 0.178$, $\gamma_{\mathrm{DIB}} \approx 0.072$). (*c*) A schematic of the NSH-type bifurcation of the admissible equilibrium $\boldsymbol{w} = \boldsymbol{w}_R^*$ (dot) and the two limit cycles $B_{1,a}$ and $B_{1,b}$. Fixed parameters in *a–c* : $\omega = 0.76$, $d = 0.95$ and $\mu = 0.15$.

and

$$\dot{\theta}_{0,-}(T, \dot{r}_{0,-}) = -\,\mathrm{Im}(q a_{22}(T))\dot{r}_{0,-}, \tag{4.11}$$

which are determined by T and $\dot{r}_{0,-}$. Note that the unbalance phase ϕ has no effect on the fixed points, i.e. it shifts the angle at impact θ_0 but does not change the nature of the dynamics. In fact, ϕ could have been scaled out of the equation. Using these values, we can check the (equivalent scaled) condition for the relative angular velocity, (2.3), to ensure that the relative angular velocity does not change at impact, and hence that we have a consistent law for the impact. The relative tangential velocity $v_{\mathrm{rel},-}$ at the contact point CP immediately before impact is given by $v_{\mathrm{rel},-} = \Omega c_{\mathrm{r}}(R/c_{\mathrm{r}} + \dot{\theta}_{i,-})$, and immediately after the impact (by applying the reset law) is $v_{\mathrm{rel},+} = \Omega c_{\mathrm{r}}(R/c_{\mathrm{r}} + \dot{\theta}_{i,+}) = \Omega c_{\mathrm{r}}(R/c_{\mathrm{r}} + \dot{\theta}_{i,-} - \mu(1+d)\dot{r}_{i,-})$. Both conditions are necessary to avoid an unphysical increase in the kinetic energy and for the three impact models (kinetic, kinematic and energetic) to be equivalent. Since $\dot{r}_{i,-} > 0$ prior to an impact, both conditions are satisfied when $v_{\mathrm{rel},i,+} > 0$, which reduces to $\dot{\theta}_{i,-} > -R/c_{\mathrm{r}} + \mu(1+d)\dot{r}_{i,-}$. Given the parameters stated earlier, and supposing that $0 < \dot{r}_{i,-} < 50$, both conditions hold in the scaled coordinates when the angular velocity $\dot{\theta}_{i,-}$ has a value greater than -40. We can see from the values given in figure 4*c*,*d* that these conditions on $\dot{r}_{i,-}$ and $\dot{\theta}_{i,-}$ are easily satisfied for all the examples considered. We can now summarize the main result concerning the period T periodic points. Let $T_{0,n,m}$ denote a zero of $F_1(T_{0,n,m})$, where $n \in \{1, \ldots, N\}$ denotes the branch pair number and $m \in \{a, b, c, d\}$ denotes the branch pair with corresponding $\dot{r}_{0,-}$ solution. The pair of largest zeros T is denoted by $n = N$, $T_{0,N,m}$, e.g $N = 1$ for $\gamma = 0.1$ (figure 4*b*). We introduce the simplified notation $\dot{r}_{0,-}(T_{0,n,m}) = \dot{r}_{0,-,n,m}$, $\theta_0(T_{0,n,m}, \dot{r}_{0,-,n,m}) = \theta_{0,n,m}$ and $\dot{\theta}_{0,-}(T_{0,n,m}, \dot{r}_{0,-,n,m}) = \dot{\theta}_{0,-,n,m}$.

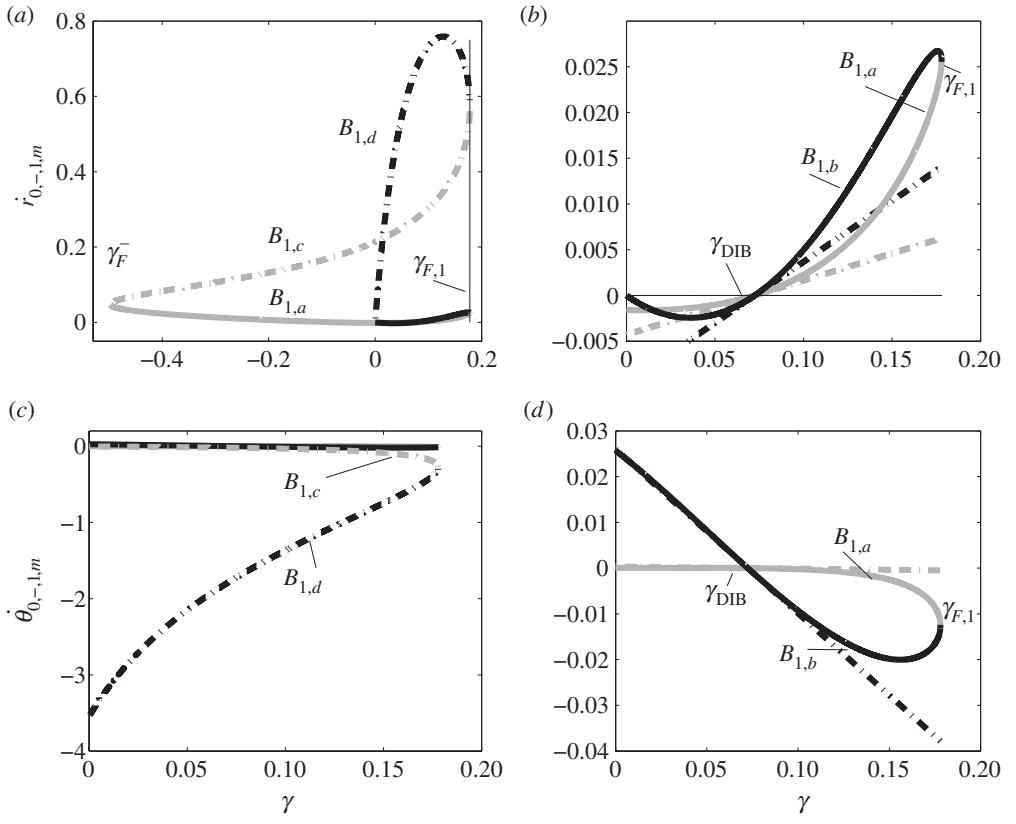

Figure 4. (*a*,*b*) Radial impact velocity of the four fixed points $B_{1,m}$. (*a*) The two fixed points $B_{1,a}$ and $B_{1,c}$ coalesce at $\gamma_F^- \approx -0.497$. Panel (*b*) is a magnification of (*a*) of the two fixed points $B_{1,a}$ and $B_{1,b}$ and now includes the respective estimate of the fixed points obtained by the local linearization of the system described in §5. ($\gamma_{\mathrm{DIB}} \approx 0.072$). (*c*,*d*) Angular impact velocity $\dot{\theta}(t-)$ of the four fixed points $B_{1,m}$ with $m = a, b, c, d$. Panel (*d*) is a magnification of (*c*) of the two fixed points $B_{1,a}$ and $B_{1,b}$ and now includes the respective estimate of the fixed points obtained by the local linearization of the system described in §5.

Proposition 4.1. *Let $n \in \{1, \ldots, N\}$ and $m \in \{a, b, c, d\}$. If there exists a period $T_{0,n,m}$ such that*

$$F_1(T_{0,n,m}) = 0$$

then there are finitely many (up to 2N), period T fixed points $B_{n,m}$ of the map P_{I} (corresponding to periodic orbits) given by

$$B_{n,m} = (T_{0,n,m}, \theta_{0,n,m}, \dot{r}_{0,-,n,m}, \dot{\theta}_{0,-,n,m}) \tag{4.12}$$

with $T_{0,n,m}$, $\theta_{0,n,m}$, $\dot{r}_{0,-,n,m}$ and $\theta_{0,-,n,m}$ determined by the equations (4.6), (4.10), (4.9) *and* (4.11), *respectively. Two pairs of fixed points, $B_{n,a}$ and $B_{n,c}$, and $B_{n,b}$ and $B_{n,d}$, have the same period, i.e. $T_{0,n,a} \equiv T_{0,n,c}$ and $T_{0,n,b} \equiv T_{0,n,d}$. If $\gamma \in (0, \gamma^*)$ then half of the fixed points, $B_{n,a}$ and $B_{n,b}$, are virtual and the other half, $B_{n,c}$ and $B_{n,d}$, are admissible.*

Proof. If the damping coefficient $\gamma > 0$ then, as stated above, $F_1(T)$ has finitely many zeros $T_{0,n,m}$. Now, let $n \in \{1, \ldots, N\}$ and $m \in \{a, b, c, d\}$. Then for each $T_{0,n,a}$ two normal impact velocities, $\dot{r}_{0,-,n,a}$ and $\dot{r}_{0,-,n,c}$ can be computed from (4.9) and hence $\theta_{0,n,a}$ and $\theta_{0,n,c}$ from (4.10) and $\dot{\theta}_{0,-,n,a}$ and $\dot{\theta}_{0,-,n,c}$ (4.11). Thus, we obtain two different periodic points, $B_{n,a}$ and $B_{n,c}$ given by (4.12), with the period $T_{0,n,a}$. For the purpose of nomenclature set $T_{0,n,c} = T_{0,n,a}$. Owing to the oscillatory character of $F_1(T)$ its zeros arise pairwise, i.e. there exists a second zero $T_{0,n,b}$. Assume that $T_{0,n,b} \neq T_{0,n,a}$ then the equivalent result follows for $B_{n,b}$ and $B_{n,d}$.

Assume $\gamma \in (0, \gamma^*)$ then $|K|^2 > 1$. Assume further that there exists a period $T_{0,n,a}$. Consider

$$\dot{r}_{0,-,n,a} := \dot{r}_{0,-}(T_{0,n,a}) = \frac{-g - \sqrt{g^2 - |q|^2|a_{12}|^2(1-|K|^2)}}{|q|^2|a_{12}|^2} < \frac{-g-|g|}{|q|^2|a_{12}|^2} \leq 0.$$

Similarly,

$$\dot{r}_{0,-,n,c} := \dot{r}_{0,-}(T_{0,n,a}) = \frac{-g + \sqrt{g^2 - |q|^2|a_{12}|^2(1-|K|^2)}}{|q|^2|a_{12}|^2} > \frac{-g+|g|}{|q|^2|a_{12}|^2} \geq 0.$$

The same holds for the period $T_{0,n,b}$. Therefore, the fixed points $B_{n,a}$ and $B_{n,b}$ are virtual but $B_{n,c}$ and $B_{n,d}$ are admissible. ■

Proposition 4.2. *Let $n \in \{1, \ldots, N\}$ and assume that the fixed points $B_{n,m}$ exist for all $m \in \{a, b, c, d\}$. Then at $\gamma = \gamma_{F,n}$ for fixed n, there are two simultaneous smooth fold bifurcations, to which the fixed points coalesce, i.e. $B_{n,a}$ and $B_{n,b}$ meet at the first fold and $B_{n,c}$ and $B_{n,d}$ at the other.*

Proof. As stated above, the function F_1 has finitely many zeros for any $\gamma > 0$ and an infinite number as $\gamma \to 0$. Furthermore, F_1 is a smooth function of γ and has regular quadratic minima. It follows, that as γ decreases, then zeros arise pairwise at regular fold bifurcations at points $\gamma_{F,n}$. Let $n \in \{1, \ldots, N\}$ and $m \in \{a, b, c, d\}$. Assume $0 < \gamma < \gamma_{F,n}$ and that the fixed points $B_{n,m}$ exist. Then there exist γ, $T_{0,n,a} \equiv T_{0,n,c}$ and $T_{0,n,b} \equiv T_{0,n,d}$ with $T_{0,n,a} \neq T_{0,n,b}$ such that

$$F_1(T_{0,n,a}, \gamma) = F_1(T_{0,n,b}, \gamma) = 0,$$

as $F_1(T)$ is oscillatory with decreasing amplitude due to $\gamma > 0$. By the continuity of $F_1(T, \gamma)$ there exists $\gamma = \gamma_{F,n}$ such that $T_{0,n,a} = T_{0,n,b} =: T_{0,n,F}$. Then for each n and $T = T_{0,n,F}$ there exist two fixed points $B_{n,a}$ and $B_{n,c}$. For $\gamma > \gamma_{F,n}$ the nonlinear function $F_1(T)$ has no zeros. Hence for each n two pairs of fixed points coincide at $\gamma = \gamma_{F,n}$, i.e. $B_{n,a}$ and $B_{n,b}$ bifurcate in a smooth fold bifurcation and so do $B_{n,c}$ and $B_{n,d}$. ■

A numerical example of the this bifurcation at $\gamma = \gamma_{F,n}$ is depicted in figures 3 and 4*a*.

We now consider the question of admissibility of the orbits. If $0 < \gamma_{F,N} < \gamma^*$ then the low impact velocity branches $B_{n,a}$ and $B_{n,b}$ are virtual for all n, whereas the other two, $B_{n,c}$ and $B_{n,d}$ are admissible by proposition 4.1. However, in the other case, $\gamma_{F,N} > \gamma^*$, further information about $\dot{r}_{0,-,n,m}$ is required. If $\dot{r}_{0,-,n,m}$ is increasing as γ is increasing then all four fixed point sets are admissible. Otherwise they are virtual. In either case, the normal velocity $\dot{r}_{0,-}$ of a pair of fixed points, $m = a, b$ or c, d, changes sign (figure 4*b*) leading one to anticipate a DIB, setting the scene for the main result of this paper. We call this a subcritical *NSH bifurcation*.

Proposition 4.3. *Let $n \in \{1, \ldots, N\}$ and assume that the fixed points $B_{n,m}$ exist $\forall m = a, b, c, d$. Assume further that $\gamma_{F,1} > \gamma^*$, and that $\dot{r}_{0,-,1,m}$ is increasing as the damping parameter γ is increasing. Then at the BEB point,*

$$\gamma = \gamma^* =: \gamma_{\mathrm{DIB}},$$

a more general DIB occurs. The limit cycles corresponding to the fixed point pairs, $B_{n,a}$ and $B_{n,b}$, clash with the admissible equilibrium $\boldsymbol{w} = \boldsymbol{w}_R^*$. As γ decreases through γ_{DIB} the three invariant sets switch from being admissible to virtual.

Proof. Let $\gamma = \gamma^*$. Then either $\dot{r}_{0,-,n,a} = 0$ or $\dot{r}_{0,-,n,c} = 0$ by (4.9). Consequently, by (4.1), it follows that

$$\boldsymbol{w}_{0,-} = -A^{-1}\boldsymbol{b} = \begin{pmatrix} K \\ 0 \end{pmatrix} = \boldsymbol{w}_{0,+}.$$

Therefore, the fixed point of P_{I} corresponds to the boundary equilibrium solution $\boldsymbol{w} = \boldsymbol{w}_{\mathrm{B}}^*$. Hence the impact velocity $\dot{r}_{0,-,n,a} = 0$ increases as γ increases from γ^*, and it undergoes a sign change corresponding to the limit cycle transitioning from physically implausible to plausible. It follows that the two limits cycles $B_{n,a}$ and $B_{n,b}$ and the admissible equilibrium $\boldsymbol{w}_R^*$ clash at the BEB point $\gamma = \gamma_{\mathrm{DIB}}$. ■

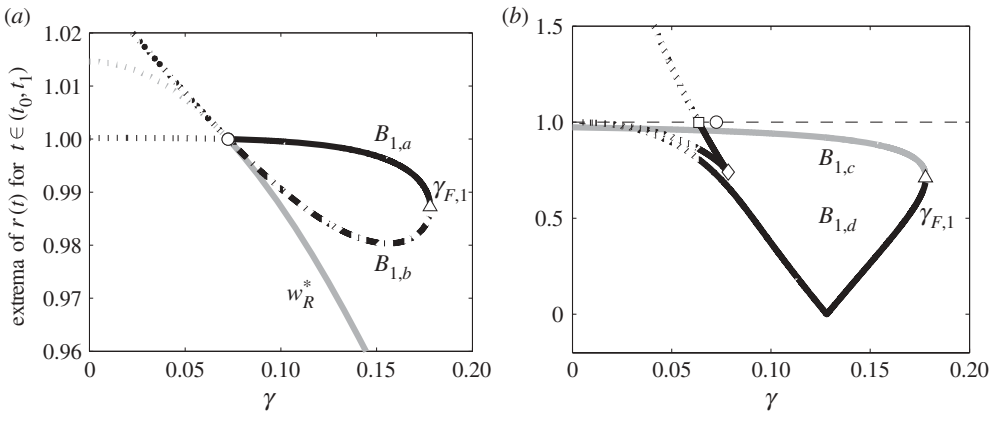

Figure 5. Bifurcation diagram of γ against local extrema of $r(t)$ for $t \in (t_0,\ t_1)$ for fixed point pairs (*a*) $B_{1,a}$ and $B_{1,b}$ and (*b*) $B_{1,c}$ and $B_{1,d}$. ($\gamma_{F,1} \approx 0.178$ (triangles)). In (*a*), we also plot the admissible equilibrium $\boldsymbol{w} = \boldsymbol{w}_R^*$ to illustrate the NSH bifurcation at $\gamma_{\mathrm{DIB}} \approx 0.072$ (circles). (*b*) depicts a grazing bifurcation at $\gamma \approx 0.0636$ (squares) after an increase in the number of local extrema of $r(t)$ at $\gamma = 0.0785$ (diamonds).

A schematic illustrating this phenomenon in (r, θ) phase space is given in figure 3*c*. Our statement is further supported by numerical examples such as figure 5*a* where the limit cycles corresponding to fixed points $B_{1,a}$ and $B_{1,b}$ are depicted. Their amplitudes, $\min(r(t))$ between impacts at times t_i and t_{i+1}, increase as γ decreases and clash with the admissible equilibrium $\boldsymbol{w} = \boldsymbol{w}_R^*$. Although we have identified under what conditions pairs of fixed points $B_{n,m}$ are admissible, their physical plausibility is not guaranteed as it is possible that between impacts the corresponding limit cycle trajectory has a further impact, figure 2*b*. Therefore, while in our global analysis we have derived the necessary existence condition for such limit cycles, further sufficient conditions are necessary as large amplitude limit cycles can undergo a grazing event [11]. In order to demonstrate whether such an impact occurs, we present the numerical analysis for our model example. We compute the trajectories of the corresponding fixed points $B_{1,m}$ and plot all local extrema of $r(t)$ between impacts $t \in (t_i, t_{i+1})$ (figure 5). The branches, $B_{1,a}$, $B_{1,b}$ and $B_{1,c}$ are not affected by this phenomenon unlike the limit cycle corresponding to the fixed point $B_{1,d}$. As γ is decreased, a grazing event [11] (orbit lies tangential to Σ with zero normal impact velocity) occurs, i.e. amplitude $r(t)$ crosses the impact surface when $\gamma = \gamma_{\mathrm{graze}} \approx 0.0636$ (figure 5*b*). Furthermore, these numerical calculations indicate that fixed point pairs with high normal impact velocity, $B_{n,c}$ and $B_{n,d}$ with $n > 1$, are virtual. To see this, note that as n increases T increases allowing more time for the orbit to exceed the impact surface, which leads to a virtual orbit, [42]. In §5, we extend this result using a local linearized system to give more precise results.

(a) Stability analysis

We present a stability analysis of the limit cycles considered as fixed points of the impact map P_{I}. In particular, we focus on the first pair of fixed points, i.e. $B_{1,m}$ with $m = a, b, c, d$, as these are the only physically plausible cases, as shown earlier in this section. Their stability is determined by the eigenvalues $\tilde{\lambda}$ of the Jacobian matrix of P_{I} given (in polar form) by

$$J(B_{1,m}) = \frac{\partial(\theta_1, \dot{r}_{1,-}, \dot{\theta}_{1,-})}{\partial(\theta_0, \dot{r}_{0,-}, \dot{\theta}_{0,-})}.$$

As P_{I} has a relatively simple analytic form, this matrix can be calculated explicitly and its eigenvalues evaluated numerically. In figure 6*a*, we present $\max(|\tilde{\lambda}|)$ of the four fixed points illustrating that $B_{1,a}$, $B_{1,b}$ and $B_{1,c}$ are unstable for all γ and that $B_{1,d}$ is quasi-periodically stable for $\gamma \in (0.083, \gamma_{\mathrm{F},1})$ but unstable otherwise. Taking into account the results from this section,

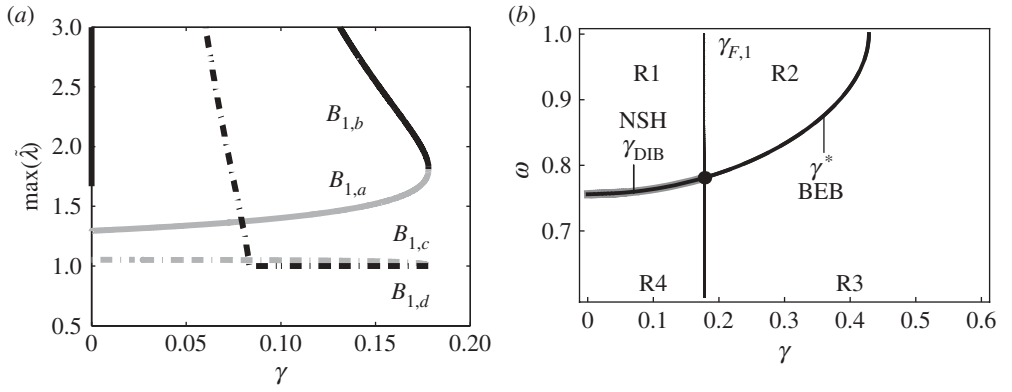

Figure 6. (*a*) Eigenvalue analysis yields one stable fixed point $B_{1,d}$ for $\gamma > 0.0834$. (*b*) Co-dimension-2 bifurcation by varying damping γ and stiffness ω. NSH signifies a non-smooth Hopf-type bifurcation.

it is evident that as γ decreases from $\gamma_{F,1}$ the fixed point $B_{1,d}$ becomes unstable before it undergoes grazing.

(b) Codimension-2 bifurcation

We complete this section with a codimension-2 bifurcation analysis studying the coalescence of various bifurcation points. Of interest is the influence of other parameters on the NSH-type bifurcation. Certain TDB parameters are constrained due to the system's characteristics such as coefficient of friction, μ, or restitution, d, which are governed by material properties. Magnetic bearing stiffness, however, can be more easily adjusted through the PID control. Hence we have chosen ω to be the second bifurcation parameter. For our particular example, $\mu = 0.15$, $d = 0.95$ and $\rho = 3/7$, we analyse the smooth fold at $\gamma = \gamma_{F,1}$ of the first fixed point set $B_{1,m}$ and the DIB point, $\gamma = \gamma_{\mathrm{DIB}}$, as we vary γ and ω (figure 6*b*). This shows that $\gamma_{F,1}$ and γ^* coincide at $\gamma \approx 0.178$ and $\omega \approx 0.781$, and that four critical regions can be identified:

R1: The three invariant sets $\boldsymbol{w}^*$, $B_{1,a}$ and $B_{1,b}$ are virtual, whereas $B_{1,c}$ and $B_{1,d}$ are admissible.
R2: The equilibrium $\boldsymbol{w}^*$ is virtual and no fixed points of P_{I} exist.
R3: The equilibrium $\boldsymbol{w}^*$ is admissible, i.e. $\boldsymbol{w}^* = \boldsymbol{w}^*_R$, and no fixed points of P_{I} exist.
R4: All invariant sets $B_{1,m}$ and $\boldsymbol{w}^*$ are admissible, i.e. $\boldsymbol{w}^* = \boldsymbol{w}^*_R$.

For values of γ and ω on the boundary between regions R2 and R3, the curve γ^*, a BEB is observed of the admissible equilibrium $\boldsymbol{w} = \boldsymbol{w}^*_R$. The smooth fold bifurcation of the fixed points of P_{I} is observed for values of γ and ω, which lie on the boundary between regions R1 and R2, and R3 and R4, i.e. the curve $\gamma_{F,1}$. The NSH bifurcation occurs for values on the boundary between regions R1 and R4, i.e. the curve γ_{DIB}. We note that the limit cycle corresponding to the fixed point $B_{1,d}$ undergoes a grazing event in regions R1 and R2, which is not included in figure 6*b*. Identifying this grazing set is part of future work.

5. Generalized local analysis of the Hopf-type bifurcation

The global analysis of this specific nonlinear system implies that limit cycles bifurcate in pairs at an NSH-type bifurcation from a boundary equilibrium point. We now examine this bifurcation in more detail by considering a local linearization of the system close to the bifurcation point. This allows us to perform the local analysis for a more general system, which includes that discussed in §4. The purpose of this section is twofold. Firstly, we can establish the conditions for the existence of two fixed point solutions of the impact map P_{I} with period T given by the

solutions of the equation (5.4). Secondly, we also obtain a more precise description of the local behaviour of the periodic solutions. We find that the estimates obtained by this analysis agree well with the calculations given in §4. To do this local analysis, we consider the complex linear differential equation in $\boldsymbol{w} = (u, \dot{u})$, with $u = r\exp(\mathrm{i}\theta)$, given by

$$\dot{\boldsymbol{w}} = A\boldsymbol{w} + \boldsymbol{b} \quad \text{in } |u| < \sigma \tag{5.1}$$

with $\sigma > 0$ and complex valued parameters α, β and Γ, where

$$A = \begin{pmatrix} 0 & 1 \\ -\beta & -\alpha \end{pmatrix} \quad \text{and} \quad \boldsymbol{b} = \begin{pmatrix} 0 \\ \Gamma \end{pmatrix}.$$

If $|u| = \sigma$, then a reset law is applied, which is given by

$$\dot{u}_+ - \dot{u}_- = -(1+d)(1+\mathrm{i}\mu)\,\mathrm{Re}(u^* \dot{u_-})\frac{u}{|u|^2}. \tag{5.2}$$

Our basic assumptions (derived from §4) are that there exist parameters α_0, β_0 and Γ_0 such that $|\Gamma_0/\beta_0| = \sigma$ and that the eigenvalues of the matrix A have negative real part. These conditions imply that at the critical parameters there is a stable boundary equilibrium as is the case for the magnetic bearing system problem.

We now consider the dynamical behaviour of solutions, which are small perturbations to this situation. To do this, we introduce a small real parameter ε and consider the perturbed system coefficients (5.1) with

$$\alpha \sim \alpha_0 + \varepsilon\alpha_1,\ \beta \sim \beta_0 + \varepsilon\beta_1 \quad \text{and} \quad \Gamma \sim \Gamma_0 + \varepsilon\Gamma_1$$

and the same reset law (5.2). From here onwards we use the symbol $\sim$ to denote equality up to the stated order in ε. We pose the asymptotic solution

$$u(t) \sim u_0 + \varepsilon u_1(t), \quad \text{or} \quad \boldsymbol{w}(t) = \boldsymbol{w}_0 + \varepsilon \boldsymbol{w}_1(t)$$

with $u_0 = \Gamma_0/\beta_0 = \sigma\,\mathrm{e}^{\mathrm{i}\Psi}$, defining the phase Ψ of u_0, and $u_1(t) = r_1(t)\,\mathrm{e}^{\mathrm{i}\theta_1(t)}$. At order ε

$$\dot{\boldsymbol{w}}_1 \sim A_0\boldsymbol{w}_1 + \boldsymbol{b}_1 \quad \text{in } |u| < \sigma,$$

where

$$A_0 = \begin{pmatrix} 0 & 1 \\ -\beta_0 & -\alpha_0 \end{pmatrix} \quad \text{and} \quad \boldsymbol{b}_1 = \begin{pmatrix} 0 \\ \Gamma_1 - \beta_1 z_0 \end{pmatrix}$$

and $|u| < \sigma$ becomes $|\sigma + \varepsilon r_1(t)\,\mathrm{e}^{\mathrm{i}(\theta_1(t)-\Psi)}|$ or

$$\varepsilon r_1(t)\cos(\theta_1(t) - \Psi) < 0.$$

There is an equilibrium at $u_0 = \Gamma_0/\beta_0$, $u_1 = (\Gamma_1 - \beta_1 u_0)/\beta_0$. Defining real constants c and ψ by

$$u_1 = \frac{\Gamma_1\beta_0 - \beta_1\Gamma_0}{\beta_0^2} = c\,\mathrm{e}^{\mathrm{i}\psi}$$

the equilibrium lies in the region $|u| < \sigma$, and hence is admissible, if

$$\varepsilon c\cos(\psi - \Psi) < 0.$$

In order to find a choice for ε, we look at the magnetic bearing system example, for which $\beta_0 = \omega^2 - 1 + \mathrm{i}\gamma^*$, $\beta_1 = i$, $\Gamma_0 = \rho\,\mathrm{e}^{\mathrm{i}\phi}$ and $\Gamma_1 = 0$. This leads to $-2\varepsilon\gamma^* < 0$. As γ^* is positive the equilibrium lies within the clearance circle if ε is negative. By choice of the sign of ε (and hence of Γ_1 and β_0), we may assume that

$$\cos(\psi - \Psi) < 0$$

and hence the stable equilibrium lies inside the clearance circle if $\varepsilon > 0$, but not otherwise. The question we wish to answer is what happens if $\varepsilon > 0$ in this case.

The general solution in the region $|u| < \sigma$ at order ε is

$$\boldsymbol{w}_1(t) = \exp(A(t-t_0))(\boldsymbol{w}_{1,0,+} + A_0^{-1}\boldsymbol{b}_1) - A_0^{-1}\boldsymbol{b}_1, \tag{5.3}$$

where $\boldsymbol{w}_{1,0,+} = \boldsymbol{w}_1(t_0+)$ denotes the post impact initial condition. Next, we need to find the reset law at order ε and hence consider the impact position first

$$|u(t_0)| = |\sigma\, \mathrm{e}^{\mathrm{i}\Psi} + cr_{1,0}\, \mathrm{e}^{\mathrm{i}\theta_{1,0}}| = \sigma.$$

This yields a constraint on the angle at impact

$$\varepsilon c r_{1,0} \cos(\theta_{1,0} - \Psi) = 0$$

or $\theta_{1,0} = \Psi + \pi/2$. Deriving the reset law for the impact velocity components requires a few more computations and we shall derive them in stages. Consider the right-hand side of (5.2) given by

$$\mathrm{Re}(u^*(t_0)\dot{u}(t_{0,-}))\frac{u_0}{|u_0|^2} = -\frac{\varepsilon r_{1,0}\dot{\theta}_{1,0,-}}{\sigma}(\sigma\, \mathrm{e}^{\mathrm{i}\Psi} + \varepsilon r_{1,0}\, \mathrm{e}^{\mathrm{i}\theta_{1,0}}) = -\varepsilon r_{1,0}\dot{\theta}_{1,0,-}\, \mathrm{e}^{\mathrm{i}\Psi},$$

where we have substituted for $\theta_{1,0}$. As the left-hand side of (5.2) can be expressed in the form of

$$\varepsilon(\mathrm{i}(\dot{r}_{1,0,+} - \dot{r}_{1,0,-}) - r_1(\dot{\theta}_{1,0,+} - \dot{\theta}_{1,0,-}))$$

we can now equate the real and imaginary parts of (5.2) to find the reset law at order ε

$$\dot{u}_{1,0,+} = \dot{u}_{1,0,-} + (1+d)(1+\mathrm{i}\mu) r_{1,0}\dot{\theta}_{1,0,-}\, \mathrm{e}^{\mathrm{i}\theta_{1,0}}.$$

As in the problem considered in §3, this system may have a variety of motions, possibly including chattering behaviour. However, for the purposes of our analysis, we seek solutions, which comprise a simple periodic orbit with a single impact. Thus, we look for a time of impact $t_1 = t_0 + T$ depending on the previous impact time t_0 and the limit cycle period T. As described in previous sections, such limit cycles satisfy repeatability conditions for position and velocity, given by $u(t_0) = u(t_1)$ and $\dot{u}(t_0-) = \dot{u}(t_1-)$, respectively. The equivalent conditions at order ε are

$$u_1(t_0) = u_1(t_1) \quad \text{and} \quad \dot{u}_1(t_0-) = \dot{u}_1(t_1-).$$

Substituting these into the general solution (5.3), we can obtain the impact maps P_I for the perturbed orbit by solving for the initial condition $\boldsymbol{w}_{1,0,-} = (u_{1,0}, \dot{u}_{1,0,-})$ that yields period T limit cycles

$$\boldsymbol{w}_{1,0,-} = -A_0^{-1}\boldsymbol{b} - \begin{pmatrix} a_{11}(T) & a_{12}(T) \\ a_{21}(T) & a_{22}(T) \end{pmatrix} \begin{pmatrix} 0 \\ \mathrm{i}(1+d)(1+\mathrm{i}\mu) r_{1,0}\dot{\theta}_{1,0,-} \end{pmatrix} \mathrm{e}^{\mathrm{i}\theta_{1,0}},$$

where

$$\begin{pmatrix} a_{11}(T) & a_{12}(T) \\ a_{21}(T) & a_{22}(T) \end{pmatrix} := (\exp(-A_0 T) - I)^{-1}.$$

It follows, by using methods similar to those used in §4, that we can find the period T by solving the nonlinear equation

$$F_1(T) := 1 - (1+d)\,\mathrm{Re}((1+\mathrm{i}\mu)a_{22}(T)) = 0. \tag{5.4}$$

A necessary condition for the existence of such periodic orbits is then given by the requirement that the nonlinear problem (5.4) has a solution T. Note, that such a solution will then describe a family of periodic orbits, parametrized by ε close to the bifurcation point. The period T of the limit cycle depends only on the parameters at the BEB, i.e. α_0 and β_0, and the impact parameters

μ and d. Then the other unknowns determined by T are given by

$$r_{1,0} = \frac{c(\ell_3 \cos(\psi - \Psi) - \ell_4 \sin(\psi - \Psi))}{-\ell_4}, \quad \dot{\theta}_{1,0,-} = \frac{\cos(\psi - \Psi)}{(1+d)(\ell_3 \cos(\psi - \Psi) - \ell_4 \sin(\psi - \Psi))}$$
$$\dot{r}_{1,0,-} = \frac{c \cos(\psi - \Psi)\,\mathrm{Im}((1+\mathrm{i}\mu)a_{22}(T))}{\ell_4},$$

where $\ell_3 := \mu\,\mathrm{Re}(a_{12}(T)) + \mathrm{Im}(a_{12}(T))$ and $\ell_4 := \mathrm{Re}(a_{12}(T)) - \mu\,\mathrm{Im}(a_{12}(T))$. Hence it follows that the linearized impact map P_I is given by

$$\theta(t_0) := \arg(z(t_0)) = \Psi + \frac{r_{1,0}}{\sigma}\varepsilon, \quad \dot{r}(t_{0,-}) = -\varepsilon r_{1,0}\dot{\theta}_{1,0,-} \quad \text{and} \quad \dot{\theta}(t_{0,-}) = \varepsilon \dot{r}_{1,0,-},$$

where the period $T = t_1 - t_0$ is a constant and does not depend on ε. If we let ε tend to zero then $\theta(t_0)$ tends to Ψ and both $\dot{r}(t_0-)$ and $\dot{\theta}(t_0-)$ tend to zero, clearly indicating that the limit cycle resulting from this impact map tends to the boundary equilibrium. Furthermore, as $\dot{\theta}$ tends to zero, the consistency condition (2.4) must be satisfied for suitably small ε and hence the form of the impact law is appropriate. Depending on the signs of the parameters, the normal impact velocity switches sign and hence demonstrates the transition from admissible to virtual limit cycle or vice versa giving rise to the NSH bifurcation. This linearization agrees with the global analysis from §4 (figure 4*b*). Furthermore, this is evidence that the NSH bifurcation can be approximated by a linear impact map in general.

6. Conclusion

A discontinuity-induced Hopf-type bifurcation has been shown to exist in rotating machines that may experience impact and friction between a rotor and TDB under contact conditions. Using a particular Poincaré map, the impact map, we have shown that at a subcritical NSH bifurcation, two unstable limit cycles and a stable admissible equilibrium without impact, are created and coexist. For a general linear complex system, the local analysis revealed that the impact map is linear in the bifurcation parameter indicating that this phenomenon can be expected in higher dimensional impacting systems.

Other typical impact dynamics such as grazing have been observed, which have to be studied further to see if they are a route to chaos via a period adding cascade observed in the 1*D* impact oscillators. We also conjecture that other Hopf-type bifurcations leading, for example, to torus doubling as in [15,16] could be observed in this system. The rich dynamics studied in this paper also revealed co-existing smooth fold bifurcations, which have not been reported in impacting systems.

The results have revealed a significant range of the dynamics that may be experienced in rotor/magnetic bearing systems. In practice, the dynamic responses that involve excessive contact forces should be avoided and the analytical techniques developed enable quantitative assessments to be made. It is recognized that simplifications have been made in the system modelling. Future research should be directed towards the inclusion of multi-mode rotors and the use of multiple magnetic bearings. It is also recommended that attention be paid to the uncertainties associated with the contact mechanics, which will involve finite contact zones and non-zero but finite durations of contact. The uncertainties in contact zones for multi-mode rotors are associated with the variability of the rotor flexure at the point of contact. Such analysis should be supported by experimental validation under precisely definable conditions of contact.

Acknowledgements. We are grateful to the anonymous referees for their helpful comments.

Funding statement. K.M. gratefully acknowledges the financial support of the EPSRC Doctoral Training Grant (DTG) and the University of Bath. P.G. was partially funded by EPSRC grant EP/E050441/1 (CICADA).

References

1. Schweitzer G. 2005 Safety and reliability aspects for active magnetic bearing applications—a survey. *P. I. Mech. Eng. I–J. Syst.* **219**, 383–392. (doi:10.1243/095965105X33491)
2. Leine RI, Nijmeijer H. 2004 *Dynamics and bifurcations of non-smooth mechanical systems*. Lecture Notes in Applied and Computational Mechanics, vol. 18. Berlin, Germany: Springer.
3. Leine RI, van de Wouw N. 2008 *Stability and convergence of mechanical systems with unilateral constraints*, vol. 36. Berlin, Germany: Springer.
4. Leine RI, van de Wouw N. 2008 Uniform convergence of monotone measure differential inclusions: with application to the control of mechanical systems with unilateral constraints. *Int. J. Nonlinear Mech.* **18**, 1435–1457. (doi:10.1142/S0218127408021099)
5. Stewart DE. 1997 Existence of solutions to rigid body dynamics and the Painlevé paradoxes. *C. R. Acad. Sci. Paris Sér. I Math.* **325**, 689–693. (doi:10.1016/S0764-4442(97)84784-2)
6. Moreau JJ. 1988 Unilateral contact and dry friction in finite freedom dynamics. In *CISM Non-smooth mechanics and applications*, vol. 302, pp. 1–82. Vienna, Austria: Springer.
7. Glocker C. 2001 Set-valued force laws. In *Dynamics of non-smooth systems* (ed. F Pfeiffer). Lecture Notes in Applied Mechanics, vol. 1. Berlin, Germany: Springer.
8. Brogliato B. 1999 *Nonsmooth mechanics*, 2nd edn. London, UK: Springer.
9. van der Schaft AJ, Schumacher JM. 2000 *An introduction to Hybrid dynamical systems*. Lecture notes in control and information sciences, vol. 251. London, UK: Springer.
10. di Bernardo M, Budd C, Champneys A, Kowalczyk P. 2008 *Piecewise-smooth dynamical systems: theory and applications*. Applied Mathematical Sciences, vol. 163. London, UK: Springer.
11. Nordmark AB. 1991 Non-periodic motion caused by grazing incidence in an impact oscillator. *J. Sound Vib.* **145**, 279–297. (doi:10.1016/0022-460X(91)90592-8)
12. Nordmark AB, Dankowicz H, Champneys AR. 2009 Discontinuity-induced bifurcations in systems with impacts and friction: discontinuities in the impact law. *Int. J. Nonlinear Mech.* **44**, 1011–1023. (doi:10.1016/j.ijnonlinmec.2009.05.009)
13. di Bernardo M, Budd C, Champneys A, Kowalczyk P, Nordmark A, Tost G, Piiroinen P. 2008 Bifurcations in nonsmooth dynamical systems. *SIAM Rev.* **50**, 629–701. (doi:10.1137/050625060)
14. di Bernardo M, Nordmark A, Olivar G. 2008 Discontinuity-induced bifurcations of equilibria in piecewise-smooth and impacting dynamical systems. *Physica D* **237**, 119–136. (doi:10.1016/j.physd.2007.08.008)
15. Xie J, Ding W, Dowell EH, Virgin LN. 2005 Hopf–flip bifurcation of high dimensional maps and application to vibro-impact systems. *Acta Mech. Sin.* **21**, 402–410. (doi:10.1007/s10409-005-0045-7)
16. Luo GW, Xie JH. 1998 Hopf bifurcation of a two-degree-of-freedom vibro-impact system. *J. Sound Vib.* **213**, 391–408. (doi:10.1006/jsvi.1997.1361)
17. Thompson JMT, Stewart HB. 2002 *Nonlinear dynamics and chaos*, 2nd edn. New York, NY: Wiley.
18. Leine RI, Van Campen DH. 2006 Bifurcation phenomena in non-smooth dynamical systems. *Eur. J. Mech. A Solids* **25**, 595–616. (doi:10.1016/j.euromechsol.2006.04.004)
19. Stronge WJ. 2004 *Impact mechanics*. Cambridge, UK: Cambridge University Press.
20. Li GX, Païdoussis MP. 1994 Impact phenomena of rotor-casing dynamical systems. *Nonlinear Dyn.* **5**, 53–70. (doi:10.1007/BF00045080)
21. Lu QS, Li QH, Twizell EH. 2003 The existence of periodic motions in rub-impact rotor systems. *J. Sound Vib.* **264**, 1127–1137. (doi:10.1016/S0022-460X(02)01386-X)
22. Keogh PS, Cole MOT. 2003 Rotor vibration with auxiliary bearing contact in magnetic bearing systems. I. Synchronous dynamics. *Proc. Inst. Mech. Eng. C J. Mech. Eng. Sci.* **217**, 377–392. (doi:10.1243/095440603321509676)
23. Simpson DJW, Meiss JD. 2007 Andronov–Hopf bifurcations in planar, piecewise-smooth, continuous flows. *Phys. Lett. A* **371**, 213–220. (doi:10.1016/j.physleta.2007.06.046)
24. Jeffrey MR. 2012 Three discontinuity-induced bifurcations to destroy selfsustained oscillations in a superconducting resonator. *Phys. D* **241**, 2077–2082. (doi:10.1016/j.physd.2011.05.008)
25. Simpson DJW, Kompala DS, Meiss JD. 2009 Discontinuity induced bifurcations in a model of *Saccharomyces cerevisiae*. *Math. Biosci.* **218**, 40–49. (doi:10.1016/j.mbs.2008.12.005)
26. Maslen EH, Schweitzer G. 2009 *Magnetic bearings: theory, design, and application to rotating machinery*. Berlin, Germany: Springer.
27. Bartha AR. 2000 Dry friction backward whirl of rotors. PhD thesis, ETH. Zürich, Switzerland.

28. Black HF. 1968 Interaction of a whirling rotor with a vibrating stator across a clearance annulus. *J. Mech. Eng. Sci.* **10**, 1–12. (doi:10.1243/JMES_JOUR_1968_010_003_02)
29. Childs DW. 1979 Rub-induced parametric excitation in rotors. *ASME J. Mech. Des.* **101**, 640–644. (doi:10.1115/1.3454114)
30. Childs DW. 1982 Fractional-frequency rotor motion due to nonsymmetric clearance effects. *ASME. J. Eng. Power* **104**, 533–541. (doi:10.1115/1.3227312)
31. Cole MOT. 2008 On stability of rotordynamic systems with rotor–stator contact interaction. *Proc. R. Soc. A* **464**, 3353–3375. (doi:10.1098/rspa.2008.0237)
32. Ehrich FF. 1965 Bistable vibration of rotors in bearing clearance. In *ASME, Winter Annual Meeting*, Chicago, IL, USA. ASME 65-WA/MD-1. New York, NY: ASME.
33. Ehrich FF. 1988 High order subharmonic response of high speed rotors in bearing clearance. *ASME J. Vib. Acoust. Stress Reliab. Des.* **110**, 9–16. (doi:10.1115/1.3269488)
34. Johnson DC. 1962 Synchronous whirl of a vertical shaft having clearance in one bearing. *J. Mech. Eng. Sci.* **4**, 85–93. (doi:10.1243/JMES_JOUR_1962_004_012_02)
35. Kirk RG. 1999 Evaluation of AMB turbomachinery auxiliary bearings. *ASME J. Vib. Acoust.* **121**, 156–161. (doi:10.1115/1.2893958)
36. Lawen JL, Flowers GT. 1997 Synchronous dynamics of a coupled shaft bearing housing system with auxiliary support from a clearance bearing: analysis and experiment. *ASME J. Eng. Gas Turb. Power* **119**, 430–435. (doi:10.1115/1.2815593)
37. Muszynska A. 2002 Rotor-to-stationary part full annular contact modelling. In *Proc. of 9th Int. Symp. on Transport Phenomena and Dynamics of Rotating Machinery, Honolulu, HI*, 10–14 February. Hawaii: ISROMAC.
38. Muszynska A. 1984 Partial lateral rotor to stator rubs. In *International Conference on Vibrations in Rotating Machinery*, 3rd, pp. 327–335. Heslington, UK.
39. Wang X, Noah S. 1998 Nonlinear dynamics of a magnetically supported rotor on safety auxiliary bearings. *ASME J. Vib. Acoust.* **120**, 596–606. (doi:10.1115/1.2893869)
40. Tessier LP. 1997 The development of an auxiliary bearing landing system for a flexible AMB-supported hydrogen process compressor rotor. In *Proc. of MAG 97, VA*, pp. 120–128. Boca Raton, FL: CRC Press.
41. Sun G, Palazzolo AB, Provenza A, Montague G. 2004 Detailed ball bearing model for magnetic suspension auxiliary service. *J. Sound Vib.* **269**, 933–963. (doi:10.1016/S0022-460X(03)00207-4)
42. Mora K. 2014 Non-smooth dynamical systems and applications. PhD thesis, University of Bath, UK.
43. Feng ZC, Zhang XZ. 2002 Rubbing phenomena in rotor-stator contact. *Chaos, Solitons Fract.* **14**, 257–267. (doi:10.1016/S0960-0779(01)00231-4)
44. Nordmark AB, Piiroinen PT. 2009 Simulation and stability analysis of impacting systems with complete chattering. *Nonlinear Dyn.* **58**, 85–106. (doi:10.1007/s11071-008-9463-y)
45. Nordmark AB, Dankowicz H, Champneys AR. 2011 Friction induced reversed chatter in rigid-body mechanisms with impacts. *IMA J. Appl. Math.* **76**, 85–119. (doi:10.1093/imamat/hxq068)
46. Budd CJ, Dux F. 1994 Chattering and related behaviour in impact oscillators. *Phil. Trans. R. Soc. Lond. A* **347**, 365–389. (doi:10.1098/rsta.1994.0049)
47. Bartolini G. 1989 Chattering phenomena in discontinuous control systems. *Int. J. Syst. Sci.* **20**, 2471–2481. (doi:10.1080/00207728908910327)
48. Kunze M. 2000 *Non-smooth dynamical systems*. Lecture Notes in Mathematics, vol. 1744. Berlin, Germany: Springer.
49. Biemond JJB, de Moura APS, Grebogi C, van de Wouw N, Nijmeijer H. Dynamical collapse of trajectories. *EPL Europhys. Lett.* **98**, 20001. (doi:10.1209/0295-5075/98/20001)